Perspectives of Organic and Perovskite-Based Spintronics

Alberto Privitera, Marcello Righetto, Franco Cacialli, and Moritz K. Riede*

Dedicated to Professor Karl Leo on the occasion of his 60th birthday

Spin-related phenomena in optoelectronic materials can revolutionize several technological applications in the areas of data processing and storage, quantum computing, lighting, energy harvesting, sensing, and healthcare. A fundamental boost to this promising field can be envisaged thanks to the use of two emerging materials, which have recently been receiving increasing scientific attention: organic semiconductors (OSCs) and halide perovskites (HPs). Here, the first progress in the resulting fields, organic- and perovskite-based spintronics, is reviewed, which will enable the manipulation of spin, charges, and photons in spin/optoelectronic devices. A link between these two classes of materials is created by highlighting the pros and cons of each technology, and their potential applications in new multifunctional spintronic devices are discussed. Current challenges in the field are also outlined, and convenient approaches to overcome them are proposed.

1. Introduction

Over the past 25 years, investigating and using electron spin has graduated from an arcane subject for theoretical scholars to a fundamental tenet that material scientists and engineers combine with other technologies to develop new and efficient electronic devices.[1] The technology of spintronics (or spin-based electronics), where the electron spin is used as the information carrier in addition to the charge, will pave the way to a new generation of electronic devices merging standard microelectronics with spin-dependent effects that arise from the quantum magnetic interactions.[2] This concept has several advantages with the potential to lead to increased data processing speed, decreased electric power consumption, and increased integration densities compared to conventional semiconductor

electronic devices—which are nearly at their physical limits.[3] In addition, taking advantage of spin interactions in optoelectronic devices will enable the improvement of their efficiency and/or stability (e.g., organic solar cells and organic light-emitting diodes (OLEDs)) and the development of new spin-based multifunctional devices (e.g., spin OLEDs, multifunctional organic spin-valve devices).[4,5,6,7]

A crucial milestone in the development of spintronics was the discovery of the giant magnetoresistance (GMR) effect in 1988.[8] Through the giant magnetoresistance mechanism, the operating principles of, e.g., magnetic disk drives, i.e., the collective magnetization of localized spins in ferromagnetic layers, have been replaced by the electronic conduction depending on the electron spin state, which gave rise to new devices, like magnetic random access memories (MRAMs).[9] Since this discovery, spin properties of electronic materials have been the focus of extensive research to rationalize, e.g., the spin relaxation and spin transport mechanisms in metals and in semiconductors. This increased interest has favored an unprecedented transition from basic research to industrial commercialization. As a result, the first GMR device as a magnetic field sensor was commercialized in 1994;[10] and read heads for magnetic hard disk drives were announced in 1997 by International Business Machines Corporation (IBM).[11] By delving deeper into the fundamental physics underlying spintronic devices, Stuart Parkin spurred the development of this field and ushered spintronic commercial applications. For instance, hard disk drives featuring a read head based on Parkin's discoveries dominated the market for two decades. Currently, GMR-based read heads have been replaced by something called giant tunneling magnetoresistance devices, which exploit a spintronic phenomenon where electrons tunnel through a thin insulator.[12] The swift evolution of the spintronic field has been buoyed by new emerging phenomena that hold great promise for the future of nonvolatile magnetic memories, e.g., skyrmions and chiral spin torque, which is at the basis of racetrack memories.[13,14]

Despite this great success, several open issues in the field of spintronics are yet to be addressed, for example, the successful spin injection into multilayer devices and the optimization of spin lifetimes in these structures, the transport of spin-polarized carriers across relevant length scales and heterointerfaces, the detection of spin coherence in nanoscale structures, and the manipulation of both electron and nuclear spins on sufficiently fast time scales.[15] The success of the research efforts can be guaranteed only by a thorough understanding of the fundamental spin interactions in solid-state materials as well as the role

Dr. A. Privitera, Prof. M. K. Riede
Clarendon Laboratory
Department of Physics
University of Oxford
Oxford OX1 3PU, UK
E-mail: moritz.riede@physics.ox.ac.uk
Dr. M. Righetto, Prof. F. Cacialli
Department of Physics and Astronomy
University College London
Gower Street, London WC1E 6BT, UK

The ORCID identification number(s) for the author(s) of this article can be found under https://doi.org/10.1002/adom.202100215.

of dimensionality, defects, and semiconductor band structure on the spin properties of materials. Although significant developments in inorganic semiconductors were achieved over the past decades (e.g., GaAs, Si, MnSe, etc.),[2] real-world applications are hindered by high cost and integration challenges, such as high temperature processing and lattice-matching requirements.

Hence, the development of new materials with tailored spin properties for efficient spin injection and spin transport is urgently needed to obtain new multifunctional spintronic devices operating at room temperature (RT). Crucially, RT operation is the vision of spintronics. Emergent new classes of optoelectronic materials that combine low-temperature and inexpensive roll-to-roll manufacturing (similar to newspaper printing or crisp package production), lightweight, color tunability, transparency, and mechanical flexibility, have catalyzed the interest of the scientific community and hold promise to realize this vision.[16]

Among the many different emerging materials of spintronic interest, organic semiconductors (OSCs), such as small molecules or π-conjugated polymers, and halide perovskites (HPs), such as methylammonium lead triiodide (MAPbI$_3$), can be considered the most promising ones. OSCs are mainly composed of light atoms such as carbon and hydrogen, which leads to unexpectedly long spin-correlation lengths due to relatively weak spin–orbit (SO) coupling and hyperfine (HF) interaction.[17] In their seminal 2002 paper, Dediu et al. observed 200 nm spin diffusion lengths in a model "sexithiophene" oligomer.[18] In general, it is reasonable to expect that the intrinsic carbon-based nature of OSCs should make these materials encouraging for transporting spins. In addition, the weak van der Waals interactions at the basis of their structural properties are promising in terms of the possibility to discover alternative routes to manipulate the electron spin in organic molecules.[19] HPs not only achieve optoelectronic properties comparable to Si and GaAs but also display relative strong SO coupling. This enables the optical injection and detection of spins, while at least partially limiting the achievable transport. Furthermore, the peculiar symmetry and band structure of HPs open the possibility of electric field and mechanical manipulation of the spin states through the so-called Rashba and Dresselhaus SO coupling.

This perspective delves into the spin properties of these two classes of optoelectronic materials and their recent achievements in the field of spintronics with the aim of understanding both their potential and the open issues, which need to be addressed in the future years. This perspective provides a specific focus on spin/optoelectronic properties, in view of possible cheap and large-scale applications. Contextually, some advancements on magnetic field effects in OSCs and HPs are not discussed in details. We refer the interest to further excellent works in literature.[20–23] This manuscript is organized in four sections. The first section briefly reviews the fundamentals of spintronic devices, which are needed to understand the spin/optoelectronic applications of OSCs and HPs. The second section concerns the spin physics of OSCs (i.e., molecular crystals, thin films based on small organic molecules, and conjugated polymers), with a particular emphasis on spin transport properties, which are the most intriguing for this class of materials. Additionally, the most recent multifunctional spintronic devices are discussed together with their open points. The third section describes the current understanding of the spin physics in HPs and possible applications that could leverage their strong spin–orbit

coupling. Finally, the fourth section provides a final discussion of the frontier applications of OSCs and HPs, which takes into account the strengths and weaknesses of these materials and the future perspectives in view of their intriguing vacuum- or solution-processed fabrication techniques and unprecedented spin, optical, and electrical properties, which paves the way to new-generation multifunctional spintronic devices.

2. Spintronic Fundamentals

The basic mechanism for a technology aiming at processing and storing information on the basis of (mostly) electronic spin (spintronics) can be summarized in three main steps, as depicted in **Figure 1**: 1) spin injection into a nonmagnetic (NM) semiconductor, 2) spin transport across the NM semiconductor, and 3) spin detection.[2,15]

Spin injection can be achieved in three main ways, as described by Žutić et al. (Figure 1, left).[2] In so-called "optical injection," incident circularly polarized (CP) photons are absorbed and their angular momentum transferred to the electron orbital momenta of the molecules within the materials.[24] In turn, the electron orbital momentum is transferred to electron spin momentum through spin–orbit coupling interaction, thereby eventually establishing a spin-polarization. In electrical injection, the spin injector, which is usually a ferromagnet (FM), has a magnetization (M), which is proportional to the difference between the concentrations of the majority and minority spins ($n_\uparrow - n_\downarrow$) of the charge carriers. When an electric current flows from the electrode to the NM material, the current is therefore spin-polarized. The spin polarization η of the injected current (also known as spin injection efficiency) can be described by the following formula[2]

$$\eta = \left| \frac{J_\uparrow - J_\downarrow}{J_\uparrow + J_\downarrow} \right| \tag{1}$$

where $J_\uparrow$ and $J_\downarrow$ represents the current carried by the majority and minority spin species, respectively. For spin injection through an interfacial barrier, the spin injection efficiency (η_i) can be expressed as

$$\eta_i = \frac{r_F P_{\sigma F} + r_i P_{\sigma i}}{r_F + r_i + r_N} \tag{2}$$

where $P_{\sigma F}$ and $P_{\sigma i}$ are respectively the conductivity polarization (defined as $P_\sigma = \frac{\sigma_\uparrow - \sigma_\downarrow}{\sigma_\uparrow + \sigma_\downarrow}$ since the two spin species have different conductivities) of the bulk FM and the interface, and r_F, r_i, and r_N represent the effective resistance of the bulk FM, the interface, and the bulk paramagnet. The conductivity polarization of the interface ($P_{\sigma i}$) depends on the nature of charge injection from the FM. For an ohmic contact between the FM electrode and the NM semiconductor, $r_i = 0$, and $r_F \ll r_N$. Thus, $\eta_i \ll P_{\sigma F}$, which implies poor spin injection. This is the well-known conductivity mismatch problem, which hinders efficient spin injection from a FM to a NM material via an ohmic contact.[25] The problem has been mitigated by using dilute magnetic semiconductors or half-metallic FMs as spin injector.[15] In the presence of a tunnel
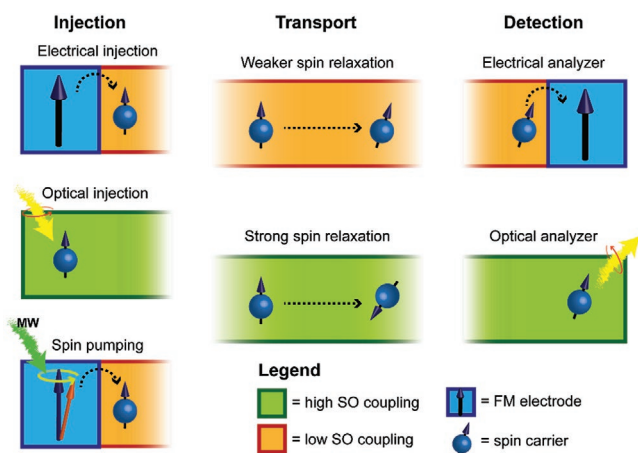
**ADVANCED
SCIENCE NEWS**
www.advancedsciencenews.com

**ADVANCED
OPTICAL
MATERIALS**
www.advopticalmat.de

Figure 1. Different experimental protocols to fabricate spintronic devices. Left: Spin injection can occur via three different techniques, namely, electrical injection from an FM material, optical injection through circularly polarized light (only in high SO coupling materials), and spin pumping by spin waves. Center: Spin polarization is lost rapidly in semiconductors with high SO coupling (e.g., inorganic materials and hybrid organic–inorganic perovskites). Conversely, spin polarization is not significantly affected in semiconductors with low SO coupling (e.g., organic materials). Right: Spin detection can occur either via FM electrodes, or via optical spectroscopy or muon resonance.

barrier, $r_i \gg r_F, r_N$, which results in efficient spin injection $\eta \approx P_{oi}$ that can be determined by the Meservey–Tedrow technique, which is based on spin-dependent tunneling from a superconducting electrode to a ferromagnet.[26] In spin pumping, demonstrated for the first time by Tserkovnyak et al.,[27] spin waves (or magnons) in FM electrodes are activated by the process of ferromagnetic electron resonance (FMR) via microwaves absorption.[28] When the induced spin waves propagate to the FM/NM interface, the magnons are either absorbed or reflected at the interface. This in turn creates a pure "spin current," i.e., not associated to charge current, in the nonmagnetic layer with spin-polarization parallel to the magnetization direction of the FM under the resonance conditions.

Following successful injection, SP carriers (or pure spin currents) diffuse across the NM material and undergo spin relaxation processes, which affect the original spin polarization of the injected spins (Figure 1, center).[29] In the solid state, the three main spin relaxation mechanisms are the SO coupling, the exchange interaction, and the hyperfine interaction, as discussed in detail below.[2,15,30] For this reason, materials that support optically generated spin polarization and therefore require high SO coupling, usually show poor spin transport properties due to fast spin relaxation promoted by SO interaction. Inorganic semiconductors and hybrid organic–inorganic perovskites are a good example of these materials. Conversely, materials with low SO coupling show longer spin relaxation times, which are essential for good spin transport properties, but do not allow generation of spin-polarization via optical techniques.[29]

Finally, spin polarization can be detected either by electrical methods or optical techniques (Figure 1, right).[31] In electrical methods, the spin detector, which again is usually a FM, provides unequal minority and majority spin concentrations ($n_\uparrow - n_\downarrow$) and preferential transmission of different spins. In

the simplest case where the detector transmits only the spins that are parallel to the magnetization of the detector, the transmission probability (T) of an electron through the detector is proportional to cos $2\theta/2$, where θ is the angle between the spin orientation of the electron arriving at the detector interface and the magnetization of the detector. This results in high T (and small device resistance), when the spin injector has parallel magnetization with respect to the detector and low T (and high resistance) if antiparallel. This behavior is at the basis of the GMR effect.[19,32] A similar result but with opposite outcome can be observed in the case of the "inverse spin valve effect" where one of the FMs preferentially transmits (injects or detects) minority spins. Finally, for the special case where the spacer is thin enough to allow spin-polarized carriers to tunnel directly through it, tunneling magnetoresistance (TMR) effect is observed, which is described well by the Jullière formula: $\frac{\Delta R}{R} = \frac{2P_1 P_2}{1 - P_1 P_2}$, where $\Delta R = R_{ap} - R_p$ (R_{ap} = resistance when the FM electrodes have antiparallel magnetization; R_p = when they have parallel magnetization), R the electrical resistances and P_1 and P_2 are the spin polarizations of the density-of-states (DOS) at the Fermi level of the two FM electrodes.[32,33] Another recently developed electrical detection approach is based on the inverse spin Hall effect (ISHE).[34,35] Here, the pure spin current J_S generated by spin pumping is converted to a charge current J_c into a FM electrode layer and generates an electromotive force $E_{ISHE} \propto J_S \times \sigma$, where σ is the spin polarization vector.[36,37] Furthermore, the spin polarization can be detected optically in materials with strong SO coupling and J-degenerate excited states. The selective occupancy of m_J sublevels by spin-polarized carriers allows the coupling of these carriers with circularly polarized photons. Hence, the helicity of the emission from these systems can be used as a probe for the presence of spin-polarized carriers. Alternatively, as summarized by Sanvito,[31] spin polarization can also be detected by using alternative techniques, such as optically detected magnetic resonance (ODMR),[38] and two-photon photoemission (TPPE),[39] or low-energy muon spin rotation (μSR) spectroscopy.[40]

3. Organic Semiconductors

OSCs are a class of carbon-based materials, which has already demonstrated to be a game-changer for optoelectronic applications, such as displays, and holding significant promises also for sensing, healthcare, and renewable energies thanks to their low-cost and low-temperature processing, as well as their favorable physical properties that enable semitransparent and flexible devices.[16,41–43] The two most investigated categories of OSCs for device applications are: 1) small semiconducting organic molecules and 2) semiconducting polymers.[44] Differently from their inorganic counterparts, both these classes are characterized by a small overlap between the π-conjugated electronic states of adjacent molecules and a strong coupling between the electronic and structural dynamics.[45] For this reason, while in inorganic semiconductors the charge carriers can be delocalized along the entire crystal and be mathematically described by Bloch wavefunctions, for most OSCs (at least those with low or moderate mobilities), charge carriers are

**ADVANCED
SCIENCE NEWS**
www.advancedsciencenews.com

**ADVANCED
OPTICAL
MATERIALS**
www.advopticalmat.de

often described as "polarons" and are localized, strongly coupled with molecular vibrational modes and sluggishly moving by thermally assisted hopping.[46–48] The strong localization of electronic states in OSCs has hindered the simultaneous control over both the energy levels and Fermi level for years. Recent studies, however, demonstrated that this can be obtain by taking advantage of molecular quadrupole moments, thereby paving the way to the possibility of band structure engineering in OSCs.[49–51]

From a spintronic perspective, the presence of light atoms, such as C, H, N, and O, gives rise to longer spin relaxation times, as a result of the weak spin-scattering mechanisms.[4,19,31] This is a fundamental requirement to achieve excellent spin transport properties and is one of the main reasons why OSCs are considered a highly promising material also for spintronic applications.[17]

3.1. Spin Transport

The factors affecting spin transport performances in OSCs can be rationalized by the Einstein's relationship, $\lambda_s = \sqrt{(D_{hop} + D_{ex})\tau_s}$, where λ_s is the spin diffusion length, D_{hop} is the diffusion coefficient for spin transport following hopping mode, i.e., phonon-assisted tunneling, D_{ex} is the diffusion coefficient for spin transport following exchange coupling mode, and τ_s is the spin relaxation time.[29] Hopping spin transport usually occurs at low charge carrier concentrations, where charge and spin transport are inextricably linked together.[52] In contrast, the exchange coupling regime occurs at high concentrations of charge carriers, which can be achieved via the impurity band or molecular doping.[53,54] The exchange coupling mechanism provides faster spin diffusion compared to hopping transport since in this regime the spin transport is decoupled from charge transport, as further discussed below.[54]

The validity of Einstein relationship in disordered OSCs has been investigated both experimentally[55] and theoretically.[56] Specifically, by studying the diffusion-driven currents of single-carrier diodes, it has been demonstrated that the relation is violated only under nonequilibrium conditions due to deeply trapped carriers. These deep trap states are discharged by charge recombination in double-carrier devices (e.g., OLEDs and OSCs), where the relationship has been unambiguously proven in thermal (quasi)equilibrium conditions. It follows directly from Einstein's relationship that in order to achieve good spin transport in OSCs, both good charge transport and long spin relaxation times are needed. In the following, these two fundamental aspects of OSCs are described and the open points discussed.

3.1.1. Spin Relaxation Mechanisms

In OSCs, the three solid-state magnetic interactions mentioned in Section 2—namely, SO coupling, exchange interaction and HF interaction—give rise to four spin relaxation mechanisms, which are depicted in the upper part of **Figure 2**.

The SO coupling is the interaction between the electron spin and its orbital motion around the nucleus.[57] For hydrogen-like atoms, SO coupling strength is proportional to Z^4 where Z is

the atomic number of the atom. This is the reason why OSCs, which comprises light-weight elements (such as C, H, O, and N), have demonstrated extremely long spin relaxation times up to milliseconds experimentally and potentially even up to seconds according to theory.[36,58] In the general case, SO coupling can be derived from the Dirac Hamiltonian[59]

$$\widehat{H}_{SO} = \frac{e\hbar}{4m^2c^2}\left[\nabla V \times \widehat{\mathbf{p}}\right] \cdot \widehat{\sigma} \tag{3}$$

where m and $-e$ are the mass and the charge of the electron, respectively, $\widehat{\sigma}$ is the Pauli spin matrix, $\nabla V(\mathbf{r})$ is the electric field, and $\widehat{\mathbf{p}}$ is the momentum operator. By comparing SO coupling strength of tris-(8-hydroxyquinoline) aluminum (Alq_3) and tris(2-phenylpyridine) ($Ir(ppy)_3$), which possess similar chemical structures, Sheng et al. showed a strong dependence of SO coupling on the atom number.[60] These studies have been further extended by Nuccio et al. by using a series of molecules resembling Alq_3 but with different metals (i.e., Ga, In, and Bi).[61] Not only the atom number but also the molecular structure has been demonstrated to influence SO coupling. For example, Yu found that the SO coupling strength in sexithiophene (T6) and copper phthalocyanine (CuPc) is lower than that in Alq_3, although the atom weight of sulfur (S) and copper (Cu) elements are higher than that of aluminum (Al).[55] This result has been rationalized by taking into account the spatial stereo-structure of Alq_3 possessing three ligands arranged orthogonally, which enhances the spin mixing and thus leads to a stronger SO coupling.

For OSCs, research efforts disclosed that the most relevant spin relaxation mechanisms related to SO coupling are the Elliot–Yafet (EY) and D'yakonov–Perel (DP) mechanisms. The EY mechanism arises from the momentum scattering of charge carriers.[59] This scattering event causes a transition between two states with different wavevectors, which also reorients the spin that is coupled to the electronic wavefunction by SO coupling. This mechanism was originally observed in the case of band-like transport but has been extended in the case of hopping transport in disordered organic solids.[52] The DP mechanism is dominant in systems that lack inversion symmetry.[62] In OSCs, structural inversion symmetry typically can arise from microscopic electric fields related to charged impurities and surface states. In the rest frame of charge carriers, these electric fields transform to an effective magnetic field whose strength depends on the charge carrier's velocity because of the Lorentz's force. The collisions of the charge carriers randomize their velocity and therefore the experienced effective magnetic fields. As a result, the spins undergo different processing orientations and velocities, which promote the decay of spin polarization. It is worth noting that EY and DP mechanisms have opposite dependences on charge carriers mobilities: EY spin relaxation is inversely proportional to the carrier mobility, since slow charges are related to numerous scattering events; conversely DP spin relaxation is directly proportional to charge carrier mobilities, since higher mobilities lead to stronger effective magnetic fields.[2] Recent studies have suggested that the DP mechanism is almost certainly not dominant in OSCs due to the low SO coupling and the quasi-localized nature of polarons.[15]
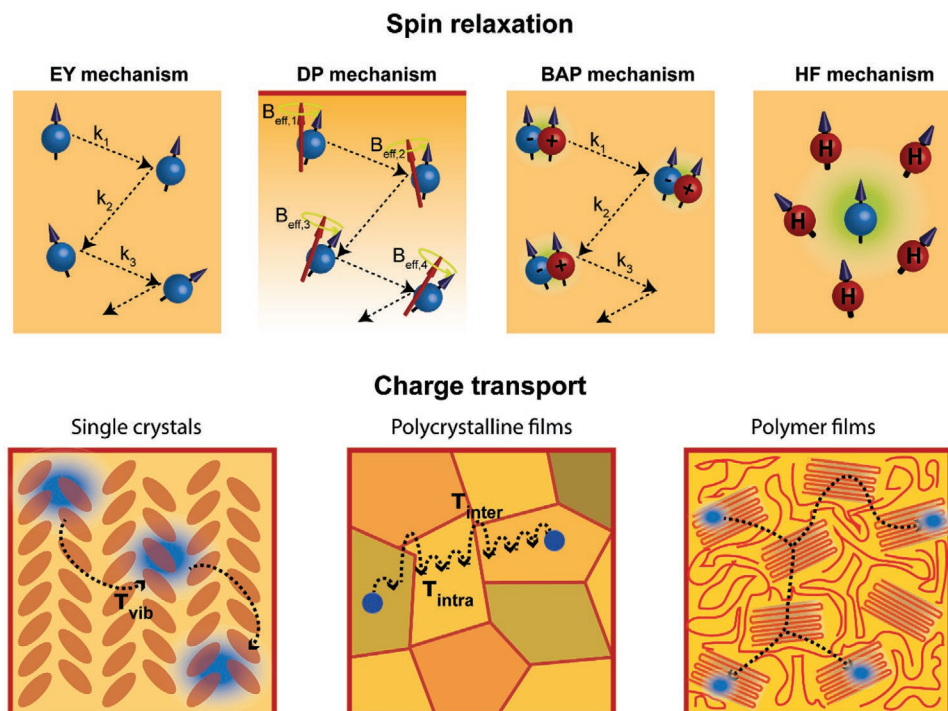
Figure 2. (Top: Spin relaxation) Schematic description of the four main spin relaxation mechanisms occurring in OSCs. From left to right: Elliot–Yafet (EY) arising from momentum scattering of charge carriers, D'yakonov–Perel (DP) arising from charged impurities and surface states, which generate magnetic fields in the rest frame of charge carriers, and Bir–Aronov–Pikus (BAP) arising from the electron–hole coupling and hyperfine (HF) mechanisms arising from the effective magnetic fields generated by the nuclear spins. (Bottom: Charge transport) Pictorial representation of the main transport mechanisms in molecular crystals, i.e., the transient localization (TL) mechanism, polycrystalline evaporated thin films, where a short-length, disorder-free intragrain transport opposes to a long-distance, disorder-limited intergrain transport, and semiconducting polymers, where charge transport is mostly hindered by energy barriers represented by amorphous regions.

The exchange interaction is the interaction between electrons in the conduction band (CB) and holes in the valence band (VB) of bipolar semiconductors, and is governed by the Hamiltonian[2]

$$\widehat{H}_{ex} = C\hat{\mathbf{S}} \cdot \hat{\mathbf{J}}\delta(\mathbf{r}) \tag{4}$$

where C is proportional to the exchange integral between the CB and VB states, $\hat{\mathbf{S}}$ is the electron-spin operator, $\hat{\mathbf{J}}$ is the hole angular momentum operator, and $\mathbf{r}$ is the relative position between electrons and holes. The exchange interaction is at the basis of Bir–Aronov–Pikus (BAP) mechanism, which in p-doped (n-doped) semiconductors is the main responsible for the spin relaxation of conduction electrons (valence holes).[63] For p-doped OSCs, when a hole spin flips due to, for example, SO interaction, the electron–hole coupling will flip the electron spin as well resulting in spin relaxation of the electrons. This process is not relevant for unipolar semiconductors, but can play a pivotal role in spin OLEDs.[64]

The HF interaction is the magnetic interaction between the spins of the electrons and the nuclei and is described by the Hamiltonian[2]

$$\widehat{H}_{HF} = \hat{S} \cdot \sum_i A_i \hat{\mathbf{I}}_i \tag{5}$$

where A_i is the hyperfine tensor, $\hat{\mathbf{I}}_i$ is the nuclei spin operator, and i the number of nuclei with which the electron spin is

coupled. HF interaction is the dominant spin relaxation mechanism for quasi-static charge carriers, i.e., when carriers are strongly localized in space like in OSCs. The HF mechanism is caused by the effective magnetic field generated by the nuclear spins, which interact with the electron and result in spin relaxation. In OSCs, there are several isotopes that possess spin nuclei, but the most relevant ones are the hydrogen atoms (1H, abundance >99.98%, $I = 1/2$). An effective way to control the HF interaction strength has been shown, e.g., by Yu et al. who replaced H by D via deuteration in poly(dioctyloxy)phenylenevinylene (DOO-PPV).[65] The substitution has decreased the effective HF field by a quarter. Another example of the important role that HF interaction plays in spin transport is described by Nguyen et al. who designed D-polymeric semiconductors where all ^{1}H near the carbon backbone have been replaced by [2]H (D) atoms, which maintains the electronic properties while changing the nuclear magnetic moment.[38] All devices based on the D-polymer showed an improved spin valve effect and longer spin diffusion lengths in agreement with the increase of the spin-relaxation time they measured.

3.1.2. Charge Transport

The maximum charge carrier mobility observed in OSCs has increased very significantly in the last decades starting from 10^{-6} to 10^{-5} cm^2 V^{-1} s^{-1} of the first organic field effect transistor

(OFET) devices to >1–10 cm^2 V^{-1} s^{-1} for the latest materials.[44] Specifically, very high mobilities have been reported for crystals since early 2000,[66] and recently even solution-processed films reported exceptional results up to ≈43 cm^2 V^{-1} s^{-1}.[67] In the following, the three main types of organic materials relevant for spintronic applications and their main charge transport mechanisms are discussed (bottom part of Figure 2). Further reviews of charge transport in OSCs can also be found in literature.[44]

Molecular Crystals: Molecular crystals, with perfect crystal structure, low defect densities, and no grain boundaries exhibit unique transport properties, arising from both their molecular structure and the packing of the individual molecules.[66,68] In molecular crystals showing the highest carrier mobilities, some transport properties are reminiscent of band-like transport, namely, ideal Hall signature and inversely proportional trend of the carrier mobility as a function of the temperature.[69–71] At the same time, optical spectroscopy shows that the electronic states of the carriers in molecular crystals are not spatially fully delocalized Bloch electrons.[72,73] To describe these observables, Fratini et al. developed an original regime of transport called transient localization (TL) mechanism.[74] This model predicts a marked tendency of the electron wavefunction to localization at short times <1 ps. This localization is due to the large thermal vibrations of the constituent molecules, which enable quantum microscopic processes. The TL model also predicts that to achieve high carrier mobilities, both the energetic disorder and the anisotropy of the band structure should be engineered.[75] Specifically, charge transport is commonly found improved in systems with isotropic distribution of transfer integrals, such as in the herringbone packing. An exception to this rule is rubrene, which shows slipped π-stack packing and remains one of the molecules with the highest reproducible mobility (>15 cm^2 V^{-1} s^{-1}).

Together with excellent charge transport, the latest results by Tsurumi et al. have shown that organic single crystals can also achieve spin diffusion lengths approaching approximately μm even at room temperature due to the coexistence of ultralong spin coherence times and relatively high band-like mobility.[76] Despite these excellent spin transport properties, molecular crystals still show some drawbacks for spintronic applications.[19] Specifically, the evaporation of magnetic electrodes on top of molecular crystals represents a serious problem due to the very high temperatures of the process, which strongly damages the organic crystal at the interface. To overcome this issue, Sun et al. have demonstrated promising results by using buffer layer assisted deposition (BLAG) and liquid nitrogen cooling methods.[77,78] Although many technological and scientific challenges still need to be addressed, spintronic devices based on an organic single crystal are a novel research field showing strong promise.

Evaporated Thin Films of Small Molecules: Since the very first observation of GMR in Alq$_3$,[77] a variety of evaporated thin films based on OSCs have been applied as spin-transport layer in spintronic devices. Different from molecular crystals, evaporated thin films usually show more defects and grain boundaries, which separate the packed crystalline domains and represent the main obstacle to the charge transport.[79] Evaporated polycrystalline films are therefore characterized by two different charge transport domains: a short-length, disorder-free intragrain transport, which opposes to a long-distance, disorder-limited intergrain transport characterized by larger energy barriers.[80,81] In recent years, several novel high-mobility OSCs (>5 cm^2 V^{-1} s^{-1}) and feasible methods for achieving high-performance charge carrier have been discovered. In particular, morphology control appears pivotal for reducing both the number of grain boundaries and their energy barriers. The most effective methods consist in the control of the chemical structure and weight of the evaporated molecules, the use of templating techniques and the application of solvent and thermal annealing.[82]

As for spintronic applications, it was found that spin transport is negatively affected not only by the grain boundary density but also by the film thickness. In addition, recently, Sun et al. demonstrated that the homogeneous amorphous OSC thin films may possess much better spin transport performance by excluding the negative effect of grain boundary density in thin film spin valves.[83] All in all, we believe that the control of grain size and mutual grain orientation by working through the numerous degrees of freedom of thermal evaporation represent the most effective way to boost spin transport in evaporated thin films.

Solution Processed Films of Conjugated Polymers: The discovery of rigid, fused-ring (D–A) copolymers with alternating electron-rich and electron-deficient units has thrust conjugated polymers into the limelight of scientific research thanks to their great OFET mobilities >5 cm^2 V^{-1} s^{-1}.[45,84] This groundbreaking achievement can be understood by taking into account the different length scales of charge transport in semiconducting polymers.[85]

At short molecular scale (<10 nm), charge carriers in high mobility polymers delocalize and move along the conjugated polymer chains very rapidly. Eventually, however, charge carriers have to move from chain to chain due to the occurrence of chain ends or kinks that act as structural traps. By using different techniques, local transport along single chains has been estimated to be orders of magnitude larger than that measured over macroscopic distances by characterizing electronic devices.[86] For example, on-chain mobilities of ladder-type polymers have recorded values as high as 600 cm^2 V^{-1} s^{-1}.[87] At mesoscale (10–100 nm), the intermolecular arrangement of polymer chains plays an important role to create transport paths, which govern charge mobility. Specifically, in semicrystalline microstructures, charges are mostly confined to the ordered regions, due to their longer conjugation length and increased intermolecular coupling. Different crystallites are usually connected by amorphous regions, which represent zones where charge transport is inherently much slower.[88] Thus, traversing amorphous regions represents a bottleneck for charge transport due to the high activation energies experiences for intercrystallite jumps. It is then important to have good connections between crystalline regions that could be rigid polymer chains, which are acting as a bridge.[89] Under these conditions, charges can effectively travel from crystal to crystal without experiencing significant impediments due to the amorphous intercrystallite regions. At larger length scales (>100 nm), charge transport is always hindered by energy barriers represented by amorphous regions between crystallites and by the mismatch between the crystallite's preferential directions. Thus, to reach high

mobilities crystallites having similar directions of the polymer backbones are preferred, since they provide favorable transport pathways for charges.[90]

As for spin transport, it has recently been discovered that polaron spin lifetimes in high-mobility conjugated polymers are governed by the charge hopping mechanism at low temperatures, whereas an EY-like relaxation where spatial scattering replaces momentum scattering is responsible for spin relaxation at higher temperatures.[52] In this regime, charges and spins are intimately related to one another, and their dynamics depends sensitively on the local conformation of polymer backbones and the crystalline packing of the polymer chains. At high spin concentrations (around 10^{20} cm^{-3}), however, spin diffusion can be decoupled by charge transport due to the exchange interaction.[54] As a result, long spin diffusion lengths of more than 1 μm and fast spin transit times through the polymer chains of around 10 ns have been demonstrated. These preliminary results suggest that further understanding of spin transport in conjugated polymers might be required (and be extremely promising) for the development of organic spintronics.

3.2. Electrical Spin Injection and Detection

Due to low SO coupling, most of the spintronic applications of OSCs are achieved through electrical spin injection and detection. In this regard, the novel frontiers of organic spintronics aim at taking advantage of the optoelectronic properties of OSCs, which have been extensively investigated in recent years, and combine them with their spin properties to obtain brand-new device functions, completely distinguished from the original ones.[91] Organic spin valves, spintronic devices where OSCs are sandwiched between two ferromagnetic electrodes, which can be independently magnetized by an external magnetic field, are considered the ideal testbed for exploiting multifunctional applications.[92] Spin valves configuration has been vastly used to develop both parallel-type functional devices, where the magnetic response is independent from the other optoelectronic properties and caused purely by the spin valve effect, and interactive-type functional devices, where the spintronic function is intrinsically coupled with other device functions and shows an interactively operating mechanism.[91]

According to the current studies, parallel-type spintronic devices have preliminarily shown their potential on multimode storage and specific sensing applications. A successful example is spin memory devices that combine the electrical memory effect with the spin-valve effect for achieving electrically controllable magnetoresistance. In this regard, Hueso et al. have reported the first hybrid spin valve based on La$_{0.7}$Sr$_{0.3}$MnO$_3$ (LSMO)/tris(8-hydroxyquinolinato) aluminum (Alq$_3$)/Al$_2$O$_3$/Co structure with electrically nonvolatile memory functionalities.[93] Despite the nice performance as electric memory, the multifunctional storage property of this device is drastically hindered by the relatively weak spin-valve effect, due to a low magnetoresistance (2%) even at very low temperature (100 K). The low magnetic resistance could be partly ascribed to the relatively low-efficiency of spin injection in the device. In fact, although LSMO has been used for years thanks to its near

100% spin polarization at low temperatures and low oxidation, which promotes its stability over time,[94,95] its spin polarization properties at room temperature are very low.[96]

Thus, improved electrodes showing better spin polarization at RT must be developed for practical application of this type of multifunctional spintronic device. This can be achieved only through the fabrication of good quality interfaces for efficient spin injection.[32] In this respect, the use of low work function metals and molecular self-assembled monolayers have shown promising results thanks to the possibility of energy band engineering, morphology control, and spin injection tuning.[97,98] In addition, organic-based magnets, which allow overcoming the problem of conductivity mismatch, have been recently proposed for device applications. The first organic FM used to fabricate a spin valve is V[TCNE]$_x$ ($x \approx 2$, TCNE: tetracyanoethylene), which possesses a high magnetic ordering temperature, a fully spin-polarized semiconducting electronic structure, chemical tunability, and low-temperature processing.[99] This has paved the way to all-organic-based spin valves whose device structure is based on two V[TCNE]$_x$ layers as injectors and detectors.[100] Examples of all-organic dual spin valve have also been reported recently using three organic spin-selective layers and introducing single molecular magnets of manganese and cobalt phthalocyanines (MnPc and CoPc) as the injector and detector.[101]

As for interactive-type functional spintronic devices based on OSCs, novel applications regarding spin storage, spin light emission, spin photovoltaic have been successfully proposed and have already commanded significant attention from the academic community. In terms of controlling the magnetic signals by applied bias, for example, Prezioso et al. obtained full electrical control on magnetoresistance of Alq$_3$-based spin valve with the possibility to adjust the spin-valve effect even into multiple states by the history of applied voltage.[102] Further examples of electrically tunable magnetic resistance have been obtained by Jiang et al.[103] and Göckeritz et al.[104] In addition, magnetoelectric coupling effects have demonstrated the possibility to achieve electrical control on magnetic signals with the introduction of a ferroelectric material between the FM electrode and the molecular spacer.[105] The ferroelectric layer generates strong interfacial dipoles as well as a built-in electric field that can be modulated by an external electric field thereby affecting the spin polarization of injected carriers.

Until now, we have discussed spin valve devices characterized by charge and spin currents, which are linked together. Recently, devices based on pure spin current, where spin angular momentum flows without the simultaneous net charge, have been investigated.[106] These pure spin devices have the potential to drastically reduce heat dissipation while storing, transmitting, and processing information.[36] Pure spin currents, usually generated by spin pumping process, have shown to be an important platform to investigate the physics of spin interactions in organic molecules and their related spintronic devices.[36] In addition, recent studies have proved that through pure-spin-current-type devices it is possible to directly probe the SO coupling strength of molecules via the inverse spin Hall effect.[107] For example, a strong SO coupling has been predicted by the great inverse spin Hall effect in C$_{60}$ films which have

ADVANCED
SCIENCE NEWS
www.advancedsciencenews.com

ADVANCED
OPTICAL
MATERIALS
www.advopticalmat.de

been rationalized considering the strong curvature of the C_{60} surface, which can induce mixing between π and σ electrons and therefore confer SO coupling to π-electrons (otherwise normally characterized by zero SO coupling).[107]

3.3. Optical Spin Injection and Detection

Although OSCs are characterized by very low SO coupling (e.g., in comparison to HPs) and therefore optical spin injection and detection is not significant, it has been experimentally demonstrated that electroluminescence (EL), photoluminescence (PL), and photocurrent can have significant responses to low magnetic fields (less than 500 mT) due to spin effects.[21] In other words, it is still possible to achieve optical spin injection and detection by taking advantage of external magnetic fields. These processes appear very promising experimental tools for a dual purpose: first, for revealing and elucidating useful excited states mechanisms occurring in organic electronic, optical, and optoelectronic devices,[108–110] and second, for leading to the development of new multifunctional organic devices with integrated electronic, optical, and magnetic properties for energy conversion, optical communication, and sensing technologies.[111]

Recent studies have indicated that most likely these magnetic field effects are mediated by intermolecular (namely, polaron pairs) and intramolecular (namely, Frenkel excitons) excited states, and their electron-spin multiplicities and spin–spin interactions.[21] Inter- and intramolecular excited states in OSCs can be either singlet ($S = 0$) or triplet ($S = 1$) spin-states which can interconvert between each other due to the HF coupling or SO coupling interactions.[112] Specifically, these internal magnetic interactions have two opposite effects. The first effect is an increase of the singlet and triplet mixing due to the spin flip mechanism, which is proportional to the HF coupling and SO coupling intensity, and the second is a decrease of spin mixing due to the internal Zeeman splitting, which increases the singlet-triplet energy difference. When an external applied magnetic field is comparable in strength to the internal magnetic interactions, the singlet–triplet conversion can be significantly affected. Most of these external magnetic field effects in organics are ascribable to intermolecular excited states since they are most likely to be influenced due to their lower internal magnetic interactions. In any case, these states can in turn affect intramolecular excited states.

An example of magnetic-field-dependent optical spin injection was already reported in 1970 by Frankevich and Sokolik who demonstrated that a low magnetic field is able to change the photocurrent of anthracene crystals.[113] This phenomenon can be readily observed also in other organic semiconducting materials[114,115] and in photoconductive polymer systems[116,117] with a modulation amplitude of about 5%. This magnetic field effect on photocurrents has been further used to elucidate not only photoexcited processes but also photovoltaic channels in organic semiconducting materials since it is an "inside-out" experimental approach to reveal detailed singlet and triplet photovoltaic processes in organic solar cells.[118] Specifically, there are two photovoltaic channels for excited states to generate photocurrent: exciton dissociation and exciton–charge interaction.[119] For the dissociation of polaron-pair states, the singlets have a larger dissociation rate relative to triplets due to their more ionic character. Conversely, the studies of phosphorescence and delayed-fluorescence quenching indicate that triplet excitons can interact more effectively with trapped charge carriers due to their longer lifetime with the final outcome of detrapping them. As a result, the major channels for the generation of photocurrent can be described by the dissociation dominated by singlets and the charge reaction dominated by triplets. By applying an external magnetic field, it is possible to perturb the singlet and triplet photoexcited states and as a result, the photocurrent through the singlet-dominated dissociation and triplet-dominated exciton–charge reaction.

As for magnetic-field-dependent optical spin detection, two main mechanisms have been envisaged in OSCs, namely, magnetic-field-dependent photoluminescence and electroluminescence.

The magnetic field dependence of photoluminescence in OSCs has been demonstrated to be mostly affected by intermolecular excited states with no significant contribution from intramolecular ones, which clearly suggests that the e–h separation distance and its related spin-exchange interaction are critical parameters.[20] At long e–h separations and weak exchange interactions, the spin interconversion becomes magnetic field sensitive and is therefore accountable for primary magnetic field effects. However, also at short e–h separation distances and strong exchange interactions, secondary magnetic field effects involving intramolecular excitonic processes have been observed in literature, for example, TTA and triplet–charge reactions.[120]

The magnetic field dependence of the electroluminescence was reported for the first time in 1975, based on time-resolved measurements, where it was demonstrated that an external magnetic field of 900 mT could reduce the delayed electrofluorescence in anthracene crystals due to the reduction of TTA under electrical excitation.[121] In later years, a positive effect of magnetic field has also been observed in Alq$_3$-based light-emitting diodes where the EL from the radiative singlet excitons was observed to increase as a function of an external magnetic field until it saturated at around 300 mT.[115] The observation has been rationalized with a positive effect of the magnetic field on the spin intermixing of polaron pairs when its strength is comparable to the internal HF field. More in general, the magnetic field can affect both spin-dependent e–h pairing and field-dependent spin intermixing in polaron-pair states. The former effect plays an important role in the determination of negative magnetic field effects at short-distance e–h capture, while the latter is the dominant mechanism responsible for positive magnetic field effects at long-distance e–h capture.[21]

All in all, despite optical spin injection and detection in OSCs not being significant, low external magnetic fields can generate strong effects, which if further understood will lead to new potential for magnetic electronic and optical devices. Specifically, spin effects in optoelectronic devices have already demonstrated great success in the field of OLEDs and showed recent interest in the field of OSCs.[5,122,123] The critical understanding of useful and detrimental excited state processes and charge transport occurring in organic electronic and optical devices will lead to improved efficiencies thereby boosting the commercialization of, e.g., organic solar cells and the development of new multifunctional opto–spintronic devices. Finally,

in recent years further carbon-based structures (e.g., carbons dots, graphene and carbon nanotubes) have been vastly investigated for their extremely intriguing optoelectronic properties, which may revolutionize the spintronic field as well.[124–127]

4. Halide Perovskites

4.1. Structure

HPs are a relatively well-known material family that received increasing attention since 2012 and was spurred by its promising photovoltaic performance. Despite some challenging issues (e.g., heavy metal and halide toxicity and poor stability),[128,129] HPs are an exciting alternative to OSCs and demonstrate excellent optoelectronic properties (e.g., long-range transport, defect tolerance, and high absorption cross-sections).[130–132] Furthermore, the possibility of reducing HPs dimensionality affords highly emitting HP counterparts, holding great promise for light-emitting applications.[133]

HPs possess the general perovskite AMX_3 chemical formula, where A is a monovalent cation, M is divalent metal ion, and X is a halide anion. A 3D network of corner-sharing $[MX_6]^{4-}$ octahedra lies at the heart of HPs optoelectronic properties. The A cation has primarily, albeit not uniquely, a geometrical role (**Figure 3**a). Few organic (e.g., methylammonium or MA, and formamadinium or FA) and inorganic (i.e., Cs) cations were found to fit the cavities of this network and afford a perovskite structure, in accordance with the Goldschmidt criterion. Such geometric criterion is partially relaxed in lower-dimensional perovskites, such as in Ruddlesden–Popper HPs or RPs. In this case, the bulkier organic cations (L) introduced form organic layers intercalated between HPs wells in a layered quasi-2D structure (Figure 3b). Here, the number of perovskite layers sandwiched between large cations layers determines the phase number n and their stoichiometric formula is $L_2A_{n-1}M_nX_{3n+1}$. 2D HPs have a phase number $n = 1$, while higher phase numbers $n > 1$ are commonly referred as to quasi-2D perovskites. Furthermore, HP nanocrystals (NCs) are another important family of perovskites with reduced dimensionality. In this case, surface ligands (e.g., oleates and alkylamines) are used to stabilize these nanocrystals with sizes in the range 4–30 nm.[134]

Among other HPs, methylammonium lead triiodide ($MAPbI_3$) emerged as the workhorse of the HPs family. Albeit still debated, this material has a tetragonal $I4cm$ symmetry and present a tetragonal-to-cubic $Pm\bar{3}m$ phase transition above 327.4 K.[135,136] At lower temperatures ($T < 162$ K), $MAPbI_3$ phase is the orthorhombic $Pnma$ phase. This transition involves the distortion (e.g., elongations and tilts) of the $[PbI_6]^{4-}$ corner sharing octahedra network. While its structure and temperature-dependent phase transitions were thoroughly characterized, the centrosymmetric nature (hence, the polar or nonpolar nature) of $MAPbI_3$ at room temperature is still a matter of debate. Its bromide counterpart $MAPbBr_3$, however, adopts a cubic $Pm\bar{3}m$ phase at room temperature and exhibit tetragonal and orthorhombic distortions at 160 and 150 K, respectively.[136] Notably, the nontrivial dynamics of the MA cation causes significant distortion to the symmetry of the lattice, further complicating this picture. As for RPs,

orthorhombic symmetry groups were reported for 2D and quasi-2D HPs. In this case, the symmetry group is dependent on the phase number n, and centrosymmetric groups were reported for $n = 1,3$ while noncentrosymmetric groups were reported for $n = 2$.[137]

4.2. Rashba and Dresselhaus Coupling

While HP optoelectronics can now be considered as a mature research field, other potential applications of HPs are being explored for applications well-beyond this realm, from photonics to spintronics (i.e., the treatment of information encoded into the "spin" magnetic moment of the charge carriers), or so-called "spin–orbitronics," e.g., the use of SO coupling in nonmagnetic materials to generate and control the spin polarized currents. The potential of HPs in spintronic (and more precisely, spin–orbitronics given the nonmagnetic nature of HPs) has been known since early 2010s and descends from the presence of lead and its high SO coupling[138,139] When inversion symmetry is not present either because of the intrinsic symmetry of the crystal unit cell, or because of defects (point, line, or surface), the SO coupling leads to a splitting of the electronic bands as a result of Rashba and Dresselhaus couplings, respectively. Dresselhaus coupling occurs in crystals lacking inversion symmetry, as Dresselhaus first demonstrated in 1955 for zinc-blend crystals.[140] The cubic Dresselhaus Hamiltonian in these systems can be expressed as

$$\widehat{H}_D \propto (\gamma / \hbar)\,\widehat{\sigma} \cdot \widehat{\varrho} \tag{6}$$

where γ is the Dresselhaus coefficient, σ is the vector of the Pauli spin matrices, and the components of ϱ are the cyclic permutation of the cubic momentum term $\varrho_x = p_x (p_y^2 - p_z^2)$, where $p_{x,y,z}$ are the component of the electron momentum vector p. Additional symmetry constrains can influence this Hamiltonian and result in additional odd-in-p terms. Interestingly, in the presence of strain along a crystallographic direction, the cubic Hamiltonian reduces to a linear form[141]

$$\widehat{H}_D \propto (\beta / \hbar)\left(\widehat{p}_x\widehat{\sigma}_x - \widehat{\sigma}_y\widehat{p}_y\right) \tag{7}$$

where β is the linear Dresselhaus coefficient, which depends on γ. Conversely, Rashba coupling depends the local source of inversion asymmetry. For an interfacial electric field along the z-direction $E = E_z\mathbf{z}$, the Rashba Hamiltonian is

$$\widehat{H}_R \propto (\alpha / \hbar)\left(\widehat{\mathbf{z}} \times \widehat{\mathbf{p}}\right) \cdot \widehat{\sigma} \tag{8}$$

As reported by Even and co-workers, for a C_{2v} system, the Rashba Hamiltonian is reduced to four terms,[142] and the resulting Rashba–Dresselhaus Hamiltonian will be

$$\widehat{H}_{RD} \propto (\alpha / \hbar)\left(\widehat{p}_x\widehat{\sigma}_y - \widehat{\sigma}_x\widehat{p}_y\right) + (\beta / \hbar)\left(\widehat{p}_x\widehat{\sigma}_x - \widehat{\sigma}_y\widehat{p}_y\right) \tag{9}$$

The resulting eigenvalue solution clearly shows the presence of a momentum-dependent energy splitting in the case of
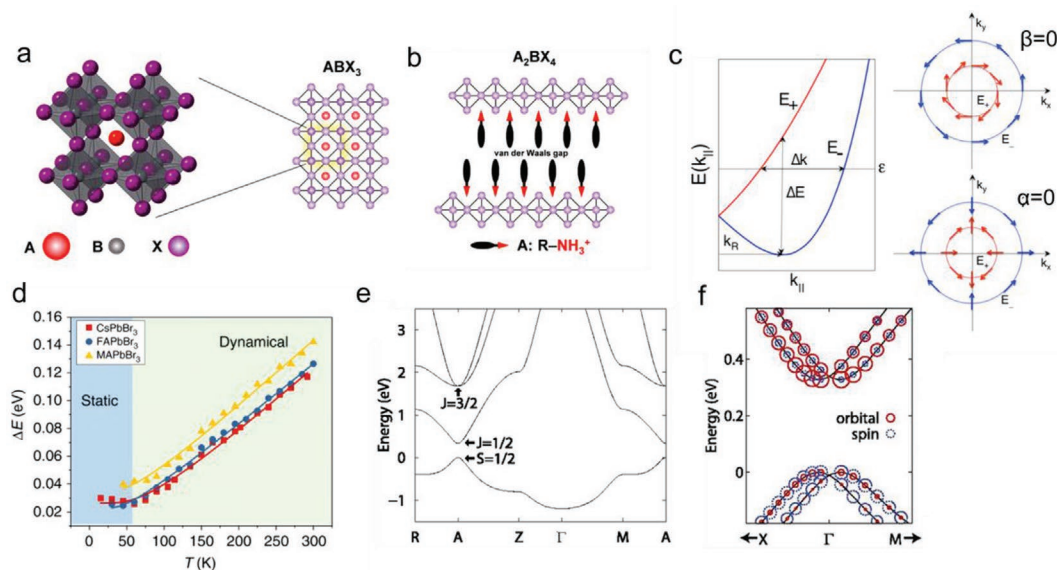
Figure 3. Schematic of the structure of a) HPs and b) RPs. Reproduced with permission.[143] Copyright 2019, American Chemical Society. c) Dispersion curves determined by Rashba–Dresselhaus Hamiltonian in a C_{2v} system and corresponding spin textures of the inner (red) and outer (blue) branches in the cases of pure Rashba or Dresselhaus coupling. Reproduced with permission.[142] Copyright 2015, American Chemical Society. d) Temperature-dependent energy splitting in lead bromide perovskite single crystals. Reproduced with permission.[144] Copyright 2019, Springer Nature. e) Tight-binding calculations of MAPbI$_3$ band structure, with indicated angular momentum and spin states, for cubic AMX$_3$ perovskite in the absence of inversion-symmetry breaking fields. f) Magnitudes of the spin and orbital (blue and red circles, respectively) angular momenta for the VBM and CBM bands in the presence of an inversion-symmetry breaking field. Reproduced with permission.[139] Copyright 2014, National Academy of Sciences.

nonzero Rashba or Dresselhaus coupling constants, as shown in Figure 3c. For a detailed derivation of these solutions, the reader is referred to the comprehensive work by Even and co-workers.[142]

The coupling constants of Dresselhaus and Rashba Hamiltonians determine the magnitude of the spin-subband splitting. Such splitting arises from the spin degeneracy lifting in the momentum space, with band-edges shifted away from high symmetry points the Brillouin zone.

Albeit with strong uncertainties on the coupling magnitude (i.e., ranging from 10^{-2} to $10\ eV$ Å), strong spin effects have been predicted computationally in 2013 for hybrid HPs. Many groups reported Rasbha values on the order of $\alpha \approx 3\ eV$ Å for MAPbI$_3$ in its tetragonal $P4mm$ phase.[139,142,145] Analogous values were reported by Neaton and co-workers for MAPbBr$_3$ and FAPbBr$_3$.[146]

In 2016, Brabec's group experimentally measured the subband splitting in MAPbBr$_3$ crystals, by angle resolved photoemission spectroscopy. And reported similar coupling constants $\alpha = 7 \pm 1$ and $11 \pm 4\ eV$ Å for orthogonal and cubic phases, respectively. Given the above mentioned centrosymmetric nature of the MAPbBr$_3$ phases and the surface sensitiveness of the employed photoemission spectroscopy, the observed band splitting in the momentum space was ascribed to Rashba SO coupling.[147] As suggested by Rakita et al. in 2017, CH$_3$NH$_3$PbI$_3$ in its tetragonal form lacks of an inversion symmetry and therefore also Dresselhaus SO coupling is expected to contribute.[135] Even though the assignment is still controversial, the presence of a dual emission peak in MAPbBr$_3$ emission spectra has been assigned to the Rashba splitting by Ehrler and co-workers.[148] Notably, the De Angelis group proposed both static and dynamic contributions to the Rashba splitting, outlining the presence of a symmetry-breaking associated with the A-cation

fluctuations.[149] Symmetry-breaking fluctuations were reported in several snapshots from molecular dynamics simulations, however, their experimental observation remains elusive.[150,151] Following observations reported by Wang et al. on MAPbI$_3$,[148] Wu et al. clarified the role of Rashba splitting in determining a dual emission peak from hybrid HP (i.e., MAPbBr$_3$, FAPbBr$_3$, CsPbBr$_3$). In these works, the formation of split spin valleys was studied through the analysis of the PL helicity at cryogenic temperatures. Remarkably, temperature-dependent studies by Wu et al. suggest that while at lower temperatures the static Rashba effect is dominant, at higher temperatures the dynamic contribution becomes significant (Figure 3d)[144] In quasi-2D HPs, first-principles calculation suggested that the Rashba effect is dependent on the layer thickness: strong Rashba splitting is estimated in noncentrosymmetric phase numbers ($n = 2$) compared to centrosymmetric ones, such as $n = 1,3$.[139] More recently, a significant Rashba coupling $\alpha = 1.6\ eV$ Å has been also reported for the Dion–Jacobson layered perovskites, a quasi-2D variant that comprises large organic dications.[152] Remarkably, the same value was estimated for 2D perovskite by Vardeny and co-workers using electroabsorption and photo-induced absorption spectroscopy.[153] Besides uncertainties on its value, the presence of Rashba coupling in HPs provides an exceptional way of manipulating spin states with zero magnetic field. Different spin control methods through the Rashba SO coupling will be explored in the next sections.

4.2.1. Electronic Band Structure

Pioneering work by Even et al. revealed through density functional theory (DFT) that the strong SO coupling is associated

**ADVANCED
SCIENCE NEWS**

www.advancedsciencenews.com

**ADVANCED
OPTICAL
MATERIALS**

www.advopticalmat.de

with reverse ordering of the band-edge electronic states and causes a CB splitting rather than a VB one.[154,155] For instance in MAPbI$_3$, CB arises from a network of Pb 6p orbitals, while the VB arises from antibonding orbitals with contributions from I 5p and Pb 6s, retaining an s symmetry. Thus, the resulting 1 eV SO splitoff affects the CB rather than the VB, conversely to what often happens for conventional group IV, II–VI, and III–V semiconductors. As further predicted by Even et al., SO interaction in lead-based HP dominates the bandgap and is reduced by two thirds when Pb(II) is substituted by Sn(II) cations, but is reinforced by heavier halogen anions.[154] The symmetry analysis of MAPbI$_3$ electronic band-edge states shows that CB is split into a lower-lying twofold degenerate E$_{1/2u}$ and a higher-lying fourfold degenerate F$_{3/2u}$ state.[155,156] On contrary, the energetics of the twofold degenerate VB is unaffected by SO interaction. This was further confirmed by Kim et al. in 2014, where a $J = 1/2$ for the CB and $S = 1/2$ for the VB was predicted using tight-binding (Figure 3e) and DFT calculations.[139]

4.3. Optical Spin Injection and Detection

4.3.1. Injection and Dynamics

As originally reported by Giovanni et al. in 2015, the Rashba and Dresselhaus splitting of the above described bands in the momentum space (Figure 3f) paves the way to optical control of spins through light helicity. According to the optical selection rules for the interaction between CP photons and this electronic band structure, CP photons selectively excite J-polarized carriers (**Figure 4**a). Authors estimated (through the consideration of Clebsch–Gordan coefficients) that such excitation generates −33% of spin polarized electrons.[157] Hence, absorption of CP light (σ^+/σ) carrying ±ℏ momentum generates up to one third of spin-polarized electrons, counterpolarized with respect to the angular momentum transferred. Implementing a CP transient absorption setup, Giovanni et al. measured the ultrafast spin polarized electrons (about 7 ps) and holes (about 1 ps) lifetimes at 77 K (Figure 4b), assigning it to EY mediated J-flip due to the observed, albeit weak, temperature dependence. Furthermore, the reported intense pump-induced Faraday rotation (FR), around 10° ± 2° µm^{-1} confirmed that it is possible to induce a giant magnetization through optical pumping of the samples.[157]

Valy Vardeny and co-workers further confirmed these observations by performing time-resolved FR on Cl-doped MAPI at cryogenic temperatures.[162] By applying a transverse magnetic field and observing quantum beatings from optical spin precession, authors were able to extract extracted g-values for electrons (2.63) and holes (−0.33). Here, liquid helium ($T = 4$ K) temperatures call into play the role of excitonic interactions in influencing the spin dynamics, which at room temperature is usually ascribed to free carriers. Belykh et al. investigated and demonstrated the role played by excitons in analogous spin coherences observed for CsPbBr$_3$.[163] An exciton g-factor $g_X = 2.35$ was extracted from the exciton Zeeman splitting observed in low temperature reflectivity measurements at $B = 10$ T. On the other hand, g-factors estimated from time-resolved FR (1.95 and 0.75 for electrons and holes, respectively)

in the same samples suggested that observed spin coherences are related to resident carriers (e.g., trapped carriers) rather than carriers involved in excitons. This findings completed the picture by Odenthal et al.,[162] where the absence of exciton exchange splitting was previously reported.

Excitonic interactions are crucial not only when considering the temperature but also the emergence of lower-dimensional and quantum confined HPs. Recently, Becker et al. explored effective mass model and group theory to describe the excitonic structure of HP NCs,[164] building on the basis set developed by Even et al. for bulk HPs.[138] Considering also the effect of crystal symmetry, calculations predicted bright emitting triplets ($J = 1$) as lower-lying states for CsPbX$_3$ NC (Figure 4c). Other reports evidenced a fine structure composed of two degenerate $|m_J = \pm 1\rangle$ states, coupled to CP light and a $|Z\rangle$ state, coupled to linearly polarized light. Although the energetics of the dark-bright exciton splitting is still debated,[158] the presence of linearly and circularly polarized bright exciton levels has been proved experimentally by using single nanocrystal and magneto-PL spectroscopy.[159,166] Leveraging this excitonic structure, many studies reported the successful injection of spin-polarized excitons and carriers into perovskite NCs for a wide variety of sizes and compositions.[159,167–169] Analogously to bulk HPs, spin lifetimes in NCs were reported to be in the ps-regime (see Figure 4d).

RP perovskites were also investigated as a viable platform to achieve the optical spin injection of perovskite. Recently, Do et al. verified the presence of an analogous excitonic substructure in 2D perovskites by low-T magneto-PL. Here, the two excitons contributing to the emission at $T = 5.9$ K exhibited linearly polarized light-emission, ascribed to the inherently strong e–h exchange. Applying a magnetic field (**B** up to 30 T) perpendicular to the perovskite basal plane, authors observed CP emission from the exciton sub-bands, saturating at about 90% for fields above 20 T.[170] Sum and co-workers harnessed this exciton substructure[171,172] (Figure 4e), by using its J-degeneracy ($m_j = \pm 1$ states) to achieve efficient optical injection of spin polarized excitons.[160] Similar to what reported for bulk HPs, circularly polarized excitation was able to generate spin-polarized exciton populations with a fast lifetime (about 240 fs). This observation was further confirmed by Beard and co-workers and extended to quasi-2D perovskites with increasing thickness.[173] Moreover, the peculiar energetic landscape of quasi-2D perovskite was exploited by Sum and co-workers to realize directional transport of the spin. Leveraging a graded structure, authors observed a transfer of spin-polarized excitons from thinner to thicker quantum well with a persistent spin polarization of about 0.5 (see Figure 4f).[161]

Across all the dimensionalities studied, the spin lifetimes were demonstrated to be not only dependent on the temperature but also on the excitonic character, on the symmetry size of the NCs/thickness of the quantum well, as well as on phonon coupling and the composition.

Zhou et al. specifically investigated effect of composition on photogenerated spin lifetime in bulk HPs using the circularly polarized pump–probe spectroscopy. At room temperature a pronounced mass effect was observed for the perovskite anion and cations: spin lifetimes were observed to increase with decreasing anions and cations masses.[174] Specifically,
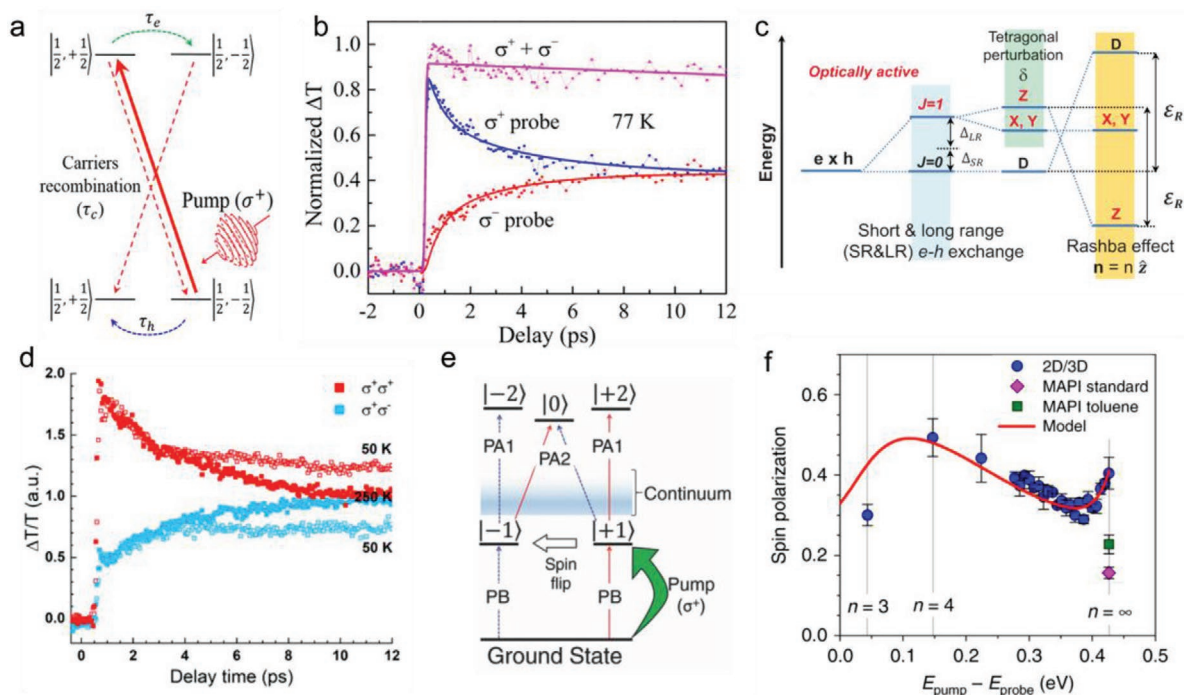
Figure 4. a) Optical selection rules for near band-edge photoexcitation in MAPbI$_3$ by CP photons angular momentum states are indicated with $|J,m_J\rangle$ where $J = 1/2$ is the electron's total angular momentum quantum number and $m_J = \pm 1/2$ is its projection in the z-axis. Absorption of a polarized pump photon raises the angular momentum by $+\hbar$ ($\Delta m_J = +1$). Reproduced with permission.[157] Copyright 2015, American Chemical Society. b) Optical spin dynamics in MAPbI$_3$ by circularly polarized pump–probe spectroscopy. σ^+ and σ^- traces represent the population of the two m_J substates. Reproduced with permission.[157] Copyright 2015, American Chemical Society. c) Exciton fine structure created by the short-range (SR) and long-range (LR) electron–hole exchange interaction, crystal field splitting, and Rashba splitting, in cube-shaped perovskite NCs with tetragonal crystal symmetry. Reproduced with permission.[158] Copyright 2019, American Chemical Society. d) Temperature-dependent optical spin dynamics in CsPbI$_3$ NCs measured by CP pump–probe spectroscopy. Reproduced with permission.[159] Copyright 2020, American Chemical Society. e) Optical selection rules for excitons and biexcitons in 2D perovskites (e.g., PEPI) with the m_J of the states labeled. Reproduced with permission.[160] Copyright 2018, Wiley-VCH. f) Exciton spin funneling in Ruddlesden–Popper (or 2D/3D) perovskites. Dots represent measured spin polarization at different energies upon polarized excitations, and line represents trap-limited spin diffusion model. Reproduced with permission.[16] Copyright 2018, Springer Nature.

the net spin lifetime was observed to decrease continuously in the MAPbBr$_x$I$_{3-x}$ from about 4 to 1 ps, with increasing iodine content. Analogous faster spin relaxation lifetimes for iodide HPs than bromide HPs were obtained by Wu and co-workers on perovskite NCs.[168] Furthermore, Wu and co-workers also deconvolved the quantum confinement effects by reporting a size-dependent characterization of the spin lifetimes. Notably, authors reported a "universal" size-dependent time constant of the k_{QE}, i.e., the component of the spin relaxation ascribed to quantum confinement. The size-dependent spin relaxation component could be described with an empirical power law $k_{QE} \propto L^{-1.19}$, where L is the size of the NC. Here, from the power law dependence of the spin lifetime decrease with decreasing size, authors deduced to a dominant surface-related contributions (expected $\propto L^{-1}$) rather than electron–hole exchange.

Differently from NCs, the thickness-dependent spin lifetime in quasi-2D perovskites was ascribed to intrinsic effects such as exciton–phonon coupling and broken symmetry effects. Thickness-dependent studies by Beard and co-workers[173] reveal that spin lifetimes thinner quasi-2D perovskites are limited to <1 ps by the strong phonon scattering. Thicker perovskite quantum wells displayed longer spin relaxation lifetimes, reaching up to 7 ps. Interestingly, symmetry breaking and the consequent enhanced Rashba effect (discussed extensively in the

next section) for quasi-2D HP with respect to bulk HPs were suggested as a crucial factor increasing the spin lifetime and counterbalancing the increased phonon scattering for lower-dimensional structures. Recently, Hall and co-workers further confirmed the role of symmetry breaking in determining the spin lifetime of quasi-2D perovskites.[175]

A variety of excitation energy, carrier density, and temperature-dependent studies tried to determine the main spin relaxation mechanism in HPs. The nature of this process is still debated in the community: while some works assign it unambiguously to EY mechanisms[157] other call into play DP mechanisms.[175,176] Notably, the paper by Belykh et al. also demonstrated the important role of carrier hyperfine interaction with nuclei in governing the spin decoherence at low temperatures and weak B-fields.[163] Given the presence of multiple intrinsic and extrinsic factors, we expect that further work will be needed to elucidate the real nature of spin relaxation processes. Crucially, Wu and co-workers reported an opposite effect of quantum confinement on CsPbI$_3$ and CsPbBr$_3$; namely, spin lifetimes were reported to be prolonged and shortened, respectively, with respect to their bulk counterparts.[168] Authors ascribed this to the negligible role of phonon scattering effects on spin lifetimes (i.e., the EY mechanism) in bromide perovskites. We envision that a better understanding of

**ADVANCED
SCIENCE NEWS**

www.advancedsciencenews.com

**ADVANCED
OPTICAL
MATERIALS**

www.advopticalmat.de

compositional and dimensional effect will be crucial to achieve a full and clear picture of the optically injected spin relaxation processes in HPs. Future research could rely on the vast amount of knowledge inherited by the studies on III–V semiconductors. It is worth to note that also for III–V the presence of multiple contributing mechanisms has been widely reported.

Comparison with GaAs and other III–V semiconductors are extremely useful for HP spintronics, since these materials provide similar opportunities in terms of optical spin injection. While the spin multiplicity of their band-edge states is different, CP light pulses can create a spin population due to similar selection rules. Notably, Maialle et al. pioneered the theory of exciton spin relaxation in GaAs quantum wells.[177] Formally akin to the BAP mechanism, they reported that two components are involved: exchange mediated spin flips and exciton scattering causing "motional narrowing." While still further work is needed to clarify the underpinning spin-relaxation mechanisms in HP, we believe that future research could widely benefit by recovering previous research on III–V semiconductor spintronics.

4.3.2. Detection

In recent years, HPs (and especially their low-dimensional counterparts) have demonstrated exceptional emission properties.[133,178] The mirror symmetry between light absorption and emission processes implies that the coupling between spin-polarized carriers and light helicity can be used not only for optical spin injection but also, in principle, for optical spin detection. Following methods already developed in valleytronics (i.e., a field where information is encoded in the electron's valley degree of freedom, by exploiting local minima or "valleys" in the electronic band structure),[179] the intensity of left and right circularly polarized PL and their ratio can be used as a probe for investigating the population of Rashba-induced spin-split bands with opposite optical helicity.

The degree of PL circular polarization or polarization ratio is defined as

$$P_R = \left| \frac{I(\sigma_+) - I(\sigma_-)}{I(\sigma_+) + I(\sigma_-)} \right| \tag{10}$$

where $I(\sigma_+)$ and $I(\sigma_-)$ represent left and right circularly polarized PL intensity under the same circularly polarized excitation. In 2018, Wang et al. reported significant P_R values (i.e., the persistence of CP light emission upon CP excitation) for both MAPbBr$_3$ and MAPbI$_3$ thin films at 77 K. Here, P_R was found to be dependent on both temperature and excitation energy excess, compatibly with the EY mechanism and the presence of hot carrier scattering and trapping. While MAPbBr$_3$ reported higher P_R values (about 1.6% under nearly resonant 532 nm excitation), MAPbI$_3$ reported much lower ones (about 0.1% under the same 532 nm). Although some discrepancy could be due to the difference in excess energies, also the different crystallographic phase should be considered. Notably, authors validated the presence of spin-polarized carriers through Hanle effect measurements. Analyzing the depolarization obtained by application of a transverse magnetic field, authors were able

to extract a spin relaxation time of about 240 ps for MAPbBr$_3$. Recently, Vardeny and co-workers reported similar results, P_R values reaching 3.1% were observed at 10 K in MAPbBr$_3$ thin films (**Figure 5**a). Here, the depolarization was found to be almost complete above 50 mT magnetic fields, thereby allowing to estimate a long spin lifetime (about 500 ps). Wang et al. presented an intuitive relation to connect P_R to the ratio between the PL lifetime τ and the spin lifetime τ_s

$$P_R \propto \left(1 + \tau / \tau_s\right)^{-1} \tag{11}$$

Following this equation, we envision that to achieve higher P_R, material development should focus on reducing radiative lifetimes (e.g., through quantum confinement, trions) without compromising on the spin lifetime. In this framework, the exceptional P_R values up to 24% at room temperature reported by Loh and co-workers for low-dimensional Dion–Jacobson perovskites could be at least partially explained by the increased radiative recombination rate (due to quantum confinement) and enhanced Rashba SO coupling.[152]

4.4. Electric Injection, Detection, and Devices

Despite its enormous potential for spin–optoelectronic devices, the injection, manipulation, and detection of spins by means of an external electric field is yet to be fully explored. Rashba effect dependence on the symmetry breaking provides an exceptional opportunity to manipulate the SO coupling in perovskites with an external field. Here, the field acts as a perturbation that lowers the symmetry of the system, and in turn affects the Rashba coefficient. In the field of III–V epitaxial semiconductor heterostructures, attempts to control the spin splitting by means of a gate voltage were reported more than 20 years ago.[180,181] Kepenekian et al. proposed and computationally estimated the electric field induced spin splitting in MAPbI$_3$ and MAPbBr$_3$. Starting from the low temperature centrosymmetric $Pnma$ phase, authors demonstrate the emergence of a significant Rashba coefficient in the valence band, up to $\alpha_{VB} \approx 0.4\, eV\,\text{Å}$. Leppert et al. reported analogous calculations on electric field-dependent Rashba coefficient for MAPbI$_3$, starting from the tetragonal $I4/mcm$ phase. In this case, a stronger field-effect was reported for the conduction band rather than the valence band, and authors estimate a $\alpha \approx 1\, eV\,\text{Å}$ for an experimentally achievable bias of 4 V on a 200 nm perovskite slab.[146]

These studies demonstrate how perovskites are extremely promising materials for spin-field effect transistor (spin-FET) devices, as originally proposed by Datta and Das in 1990. Kepenekian et al. provide a qualitative estimate that suggest the feasibility of this scheme in perovskites (Figure 5b).[142]

Notably, the experimental realization of spin–optoelectronic devices depends on the details of spin injection and transport. In this sense, the recent report by Yang et al. reported the successful room-temperature pure spin injection in MAPbCl$_{3-x}$I$_x$ by coupling spin pumping with ISHE detection in the FM electrode.[182] The pure spin transport was measured in perovskite by fabricating trilayers with Ni$_{80}$Fe$_{20}$ and Pt electrodes (Figure 5c) and reported outstanding figures for spin transport: up to 61 nm diffusion lengths and estimated electron
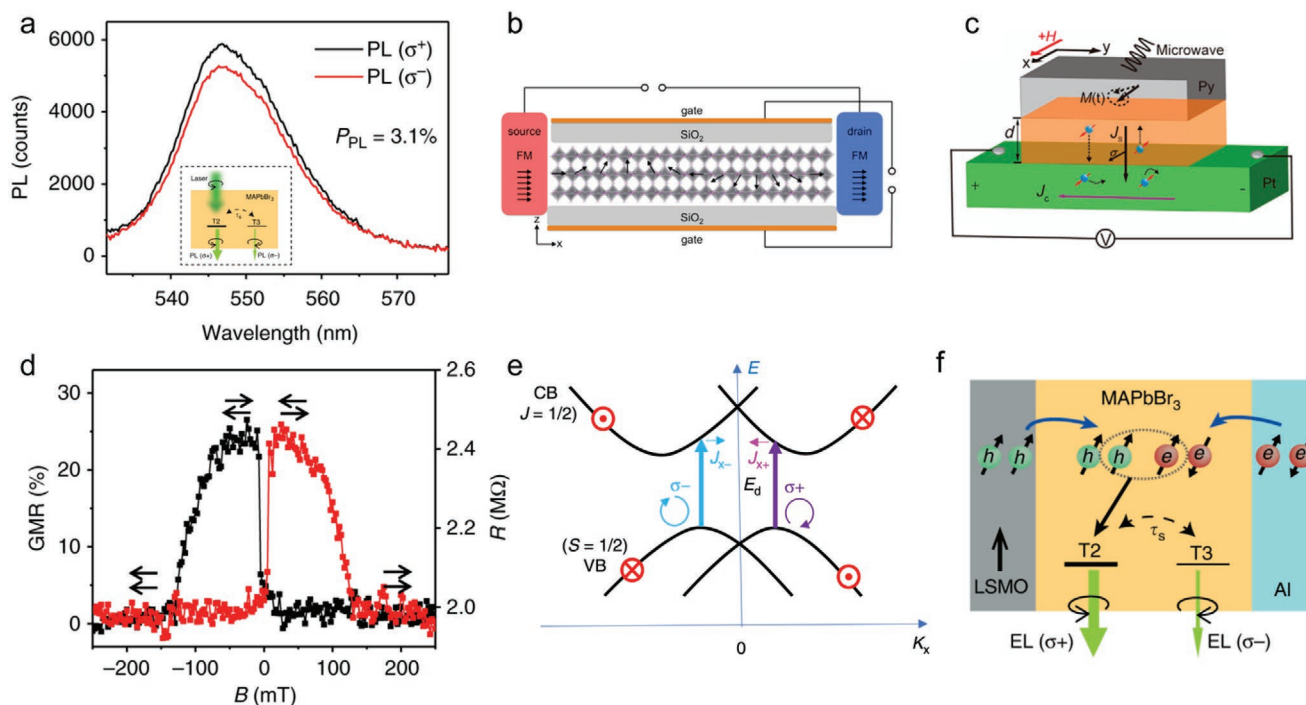
Figure 5. a) Optical spin injection and detection using CP excitation and measuring the polarization of PL emission spectra in MAPbBr$_3$ at 10 K. The resulting polarization ratio is 3.1%. Inset: A schematic of the process, where two J-polarized exciton states are excited selectively by CP light and coupled by spin relaxation. Reproduced with permission.[185] Copyright 2019, Springer Nature. b) Schematic of a perovskite-based spin-FET, following the scheme proposed by Das and Datta. Reproduced with permission.[142] Copyright 2015, American Chemical Society. c) Schematic of spin transport measurement in MAPbI$_3$ setup, which couples injection by spin pumping and ISHE detection. Reproduced with permission.[182] Copyright 2020, American Chemical Society. d) GMR response of a MAPbBr$_3$-based spin-valve measured at 10 K and applied bias voltage, $V = 0.1$ V as a function of the magnetic field. Red and black lines represent the sweeping direction of the field, and the maximum GMR observed is 25%. Reproduced with permission.[185] Copyright 2019, Springer Nature. e) Schematic of the circularly photogalvanic effect in perovskites. The absorption of CP light populates selectively the two Rashba splitted branches and generates two counterpropagating currents. Reproduced with permission.[186] Copyright 2020, Springer Nature. f) Working principle of the spin-LED. Spin-polarized holes injected by the FM anode form spin-polarized excitons, T2 that emit circularly polarized electroluminescence, and allow the optical spin detection. Reproduced with permission.[185] Copyright 2019, Springer Nature.

and hole spin relaxation times of 1.5 and 1.1 ns, respectively. In view of the strong SO coupling, such long-range spin transport was unexpected. Authors speculated that suppression of spin relaxation and electrical spin/injection could be attributable to Rashba spin splitting at grain boundaries.

While spin injection by spin pumping is known to circumvent this issue,[183] electrical spin injection from ferromagnets into diffusive semiconductors is hindered by the impedance mismatch of the two materials.[184] Notably, Vardeny and co-workers successfully demonstrated electrical spin injection from an FM electrode (LSMO) to MAPbBr$_3$ perovskite by realizing spin valves (Figure 5d). Authors reported a maximum GMR value of 25% and estimated spin lifetimes up to 1 μs at 10 K.

The circular photogalvanic effect (CPGE) is another crucial observation that not only allows verifying the presence of the Rashba SO coupling but also allows confirming the photogeneration of spin-related currents. This phenomenon combines two important spintronic properties of perovskites: i) the optical spin injection by means on circularly polarized light (see above discussion); and ii) the electrical detection of spin populations through ISHE in the perovskite material. Namely, CPGE measures helicity-dependent photocurrent by recording the

photocurrent in metal/perovskite/metal sandwich structures illuminated with circularly polarized light. As demonstrated by Vardeny and co-workers, the selective population of the two Rashba branches creates two subsets of carriers moving with opposite group velocity, when away from the band edge, and thus produces two opposite currents (Figure 5e).[186] Hence, as further demonstrated by THz emission spectroscopy, the CPGE determines the creation of ultrafast hot-carriers photocurrents.[131,187] CPGE was predicted and experimentally demonstrated for bulk MAPbI$_3$ perovskite and for 2D phenethyl ammonium lead iodide (PEPI).[186,188–190] Interestingly, the relatively large exciton binding energies in PEPI (490 meV) raise questions about the contribution of excitons to spin-dependent photocurrents. While Vardeny and co-workers suggested that this could be caused by spin-galvanic effect, we expect that future work will be needed to further clarify the possible spintronic role of excitons in 2D perovskites.[186,191]

While implementation of spin effects in perovskite devices initially concerned indirect effects of spin states, e.g., effect of light polarization on photovoltaic efficiencies and Rashba splitting effects on carrier relaxation and recombination,[148,192,193] the advancements summarized above pave the way for the realization of perovskite spintronic devices.

In 2015, Even and co-workers hypothesized and demonstrated the feasibility of a perovskite spin-FET. In this architecture, the precession of the carrier spins caused by the Rashba coupling is modulated by the gate voltage. Authors hypothesize that the absence of Rashba coupling in the absence of external electric field (due to the centrosymmetric phases considered) would make the device architecture less delicate. However, to the best of our knowledge, this architecture has not been experimentally reported yet.

Conversely, Vardeny's group demonstrated the possibility of using $MAPbBr_3$ to realize spin-light emitting diodes (spin-LEDs).[185] These devices remarkably combine what we described above as electrical spin injection and optical spin detection. Namely, the authors replaced conventional indium-doped tin oxide electrode with an FM electrode and observed the degree of circular polarization of the electroluminescence (Figure 5f). Albeit small, these effects demonstrate the feasibility of cheap and solution processed spin–optoelectronic devices.

5. Discussion and Outlook

Spintronics based on organic and HP semiconductors is a promising research field still in its infancy, which holds great potential for many technological applications, e.g., multifunctional devices combining optical, magnetic, and electronic properties. The possibility to combine spintronic properties comparable to those of inorganic semiconductors with low-cost, lightweight, mechanically flexible, and chemically engineerable fabrication paves the way to large-scale spin–optoelectronic devices fabricated by roll-to-roll techniques.[194] Although exciting developments have been reported in the past decade, many challenges are yet to be solved, both on the scientific and on the technological side. For instance, improvement of the ferromagnet/semiconducting interface are urgently needed.[32] The fragile nature of both organic and perovskite materials hinders the use of conventional microfabrication techniques and requires the development of nondestructive contacting strategies for efficient spin injection. Adoption of low work function metals and leveraging of self-assembled molecular monolayers (SAMs) are promising strategies to improve the spin-injection efficiency via energy band alignment, modification of morphology, and tuning of spin polarization at the interface between a ferromagnetic electrode and an OSC. While alternative spin injection strategies circumventing this issue (e.g., ballistic spin-carrier-injection and spin-pumping methods, described above) have also been experimentally demonstrated, we expect that future research efforts will also focus on improving electrical spin injection.

In this sense, the study of interfacial properties is a highly promising idea to boost the use of organic materials in spintronic applications. This is the realm of "spinterface engineering," where spin electronics learns from organic electronics and organic chemistry on how best to get the spins moving into interfacial structures.[195] These studies would promote prospects for spin optics, quantum computing, and nonvolatile memory. However, the full potential of this intriguing field will become apparent only after being able to control the experimental conditions sufficiently to fabricate reproducible devices.

A concerted effort is therefore needed to understand how deposition processes and conditions, postdeposition annealing treatments, film morphology, surface roughness, and impurities influence the performance of organic-based magnetic devices. Some encouraging pointers are beginning to emerge from theory, but we are still far from real technological applications.

Despite the exceptional progress summarized above, there is large space for further development on both the material and the device side.

From a material perspective, defects and impurities still remain a crucial limiting factor that hinders the spin transport in solution processed materials.[29] While HP can leverage their defect tolerance, which allow reaching approximately μm carrier diffusion lengths in routinely synthesized thin films, the strong SO coupling remains an inherent limitation. In this regard, OSCs possess weak SO coupling that potentially enables ultralong range spin transport properties (more than tens of μm). The record spin diffusion lengths reported for OSCs nowadays (>1μm) are now comparable with, if not longer than, those of inorganic semiconductors such as GaAs, Ge and Si.[54,76] However, these values were obtained for specially designed test structures, which are different from the technologically relevant spintronic devices and systems, and as such further studies are needed with architectures relevant for commercial applications. On top of this, the presence of pinholes and impurities in OSCs hinders the development of reproducible and stable organic spintronic devices. A first promising approach to improve stability of organic spin valve devices has been proposed by Dediu et al.[196] In their work, an inorganic insulator (Al_2O_3) has been inserted between the top Co electrode and the organic layer in order to slow down the interdiffusion and improve the stability of the device. However, the suppressed interdiffusion was achieved at the expense of losing some spin polarization injection capability from the Co electrode. Such a trade-off between stability and degree of spin polarization epitomizes the challenges that will need to be addressed in this field.

From a device perspective, perhaps the most fundamental question that still needs answering in organic spintronics is the absence of Hanle effect reports. Measurements of Hanle precession of spins in a magnetic field that is noncollinear with the spin quantization axis could provide unambiguous proof of spin injection in nonmagnetic materials, as demonstrated for inorganic semiconductors.[197] Riminucci et al. uncovered this issue with a work on $LSMO/Alq_3/AlO_x/Co$ spin valves with 200 nm Alq_3 layers.[198] In this work, no Hanle effect was observed, which could be rationalized only by suggesting an exceptionally high carrier mobility (30 cm^2 V^{-1} s^{-1}) resulting in a small precession angle during transit. An analogous result was observed by Grünewald et al. who investigated organic spin valves with Alq_3 (40–100 nm) and PTCDI-C4F7 (100–600 nm) spacers, and LSMO (bottom) and CoFe (top) electrodes.[199] Again, no Hanle effect could be observed, which was attributed to (multistep) tunneling via pinholes in the organic layers in combination with tunneling anisotropic magnetoresistance originating from charge injection at the LSMO/organic interface. Although the presence of the Hanle effect in OSCs would be an unambiguous proof for spin injection, failure to observe it does not rule out the possibility that spin injection takes place. Rather, these discrepancies call for a deeper understanding of spin injection and transport

in organic devices. For instance, higher magnetic fields could prove useful, as postulated by Yu,[200] to counteract a postulated exchange-induced spin-transport mechanism between localized charges. On the other hand, the Hanle effect has been reported in halide perovskites both at low temperatures and room temperature, for optical spin injection.[161–163,185] The relatively fragile nature of perovskites limits the use of photo and e-beam lithography, thus posing challenges for the measurement of the "conventional" electrical Hanle effect.[201] However, recent reports of magnetoelectroluminescence[202] and of the oblique Hanle effect by spin pumping techniques[201] pave the way for future characterization of spin injection and transport in halide perovskites.

In addition to this, the new effect named chiral-induced spin selectivity (CISS) could enable a new paradigm in the field of spin/optoelectronics.[203] This approach not only can potentially enhance the spin diffusion lengths but also allows the manipulation and control of spintronic interfaces without the need for a permanent ferromagnetic layer. Hence, CISS could afford simple nanometric and power-efficient spintronic devices where local spin currents are produced by spin-selective electron transport through chiral molecules. In addition, through the CISS effect it is possible to optically generate local spin-based magnetization even at room temperature in micrometer-sized devices.

It is worth to note that the CISS effect is not limited to OSCs. In fact, HPs in their RPs form could offer unprecedented opportunities to engineer spin transport through the CISS effect. In these low-dimensional semiconductors (Figure 3b), chiral large cations can be implemented in between the perovskite layers. The resulting chiro-optical perovskites are among the most interesting and promising advances in perovskite spintronics. A handful of papers have already demonstrated their potential: enhanced spin transport and spin-exciton formation without an external magnetic field.[204–207]

Last, this perspective describes the potentials and the issues of two different family of semiconductors: organics and halide perovskites. From the properties outlined above emerges their complementary nature. Hence, we expect that spin-engineered strategies for coupling OSCs and HPs could unlock their potential and exploit the best of both worlds. In this context, some experiments have already shown promising results arising from the coupling of HP nanoparticles and organic materials,[208] and the doping of HPs with heteroelements of spintronic interest (e.g., Mn and Fe) could open to an excited yet unexplored horizon.[209]

While studies for coupling OSCs and HPs (potentially doped) is already underway, a focusing on the spin dynamics could give a further spin to this exciting field.

Acknowledgements

Conflict of Interest

The authors declare no conflict of interest.

Author Contributions

A.P. and M.R. contributed equally to this work. The review was conceived and designed by A.P. and M.R. M.K.R. and F.C. supervised the work and contributed with fruitful discussion. The first manuscript draft was prepared by A.P. and M.R. Specifically, A.P. focused on the general introduction and the organic spintronic part and M.R. focused on the hybrid organic–inorganic perovskite section. All authors reviewed the manuscript and participated actively in its final discussion.

Keywords

[1] J. M. D. Coey, J. M. D. Coey, *Magnetism and Magnetic Materials*, Cambridge University Press, Cambridge **2010**.
[2] I. Žutić, J. Fabian, S. D. Sarma, *Rev. Mod. Phys.* **2004**, *76*, 323.
[3] J. Puebla, J. Kim, K. Kondou, Y. Otani, *Commun. Mater.* **2020**, *1*, 24.
[4] G. Szulczewski, S. Sanvito, M. Coey, *Nat. Mater.* **2009**, *8*, 693.
[5] I. Ramirez, A. Privitera, S. Karuthedath, A. Jungbluth, J. Benduhn, A. Sperlich, D. Spoltore, K. Vandewal, F. Laquai, M. Riede, *Nat. Commun.* **2021**, *12*, 471.
[6] S. Reineke, M. Thomschke, B. Lüssem, K. Leo, *Rev. Mod. Phys.* **2013**, *85*, 1245.
[7] A. J. Gillett, A. Privitera, R. Dilmurat, A. Karki, D. Qian, A. Pershin, G. Londi, W. K. Myers, J. Lee, J. Yuan, S.-J. Ko, M. K. Riede, F. Gao, G. C. Bazan, A. Rao, T.-Q. Nguyen, D. Beljonne, R. H. Friend, arXiv:2010.10978, **2020**.
[8] M. N. Baibich, J. M. Broto, A. Fert, F. N. Van Dau, F. Petroff, P. Etienne, G. Creuzet, A. Friederich, J. Chazelas, *Phys. Rev. Lett.* **1988**, *61*, 2472.
[9] G. A. Prinz, *Science* **1998**, *282*, 1660.
[10] J. Daughton, J. Brown, E. Chen, R. Beech, A. Pohm, W. Kude, *IEEE Trans. Magn.* **1994**, *30*, 4608.
[11] C. H. Tsang, R. E. Fontana, T. Lin, D. E. Heim, B. A. Gurney, M. L. Williams, *IBM J. Res. Dev.* **1998**, *42*, 103.
[12] S. S. P. Parkin, C. Kaiser, A. Panchula, P. M. Rice, B. Hughes, M. Samant, S.-H. Yang, *Nat. Mater.* **2004**, *3*, 862.
[13] S. Parkin, S.-H. Yang, *Nat. Nanotechnol.* **2015**, *10*, 195.
[14] K.-S. Ryu, S.-H. Yang, L. Thomas, S. S. P. Parkin, *Nat. Commun.* **2014**, *5*, 3910.
[15] S. Majumdar, H. S. Majumdar, R. Österbacka, in *Comprehensive Nanoscience and Technology* (Eds: D. L. Andrews, G. D. Scholes, G. P. Wiederrecht), Academic Press, Amsterdam **2011**, p. 109.
[16] O. Ostroverkhova, *Chem. Rev.* **2016**, *116*, 13279.
[17] V. A. Dediu, L. E. Hueso, I. Bergenti, C. Taliani, *Nat. Mater.* **2009**, *8*, 707.
[18] V. Dediu, M. Murgia, F. C. Matacotta, C. Taliani, S. Barbanera, *Solid State Commun.* **2002**, *122*, 181.
[19] D. Sun, E. Ehrenfreund, Z. Valy Vardeny, *Chem. Commun.* **2014**, *50*, 1781.
[20] L. Yan, Y. Wu, Z. Xu, B. Hu, *Synth. Met.* **2009**, *159*, 2323.
[21] B. Hu, L. Yan, M. Shao, *Adv. Mater.* **2009**, *21*, 1500.
[22] H. Xu, M. Wang, Z.-G. Yu, K. Wang, B. Hu, *Adv. Phys.* **2019**, *68*, 49.
[23] C. Zhang, D. Sun, C. X. Sheng, Y. X. Zhai, K. Mielczarek, A. Zakhidov, Z. V. Vardeny, *Nat. Phys.* **2015**, *11*, 427.
[24] E. J. Johnson, *J. Lumin.* **1987**, *37*, 235.
[25] E. I. Rashba, *Phys. Rev. B* **2000**, *62*, R16267.

**ADVANCED
SCIENCE NEWS**

www.advancedsciencenews.com

**ADVANCED
OPTICAL
MATERIALS**

www.advopticalmat.de

[26] R. Meservey, P. M. Tedrow, *Phys. Rep.* **1994**, *238*, 173.

[27] Y. Tserkovnyak, A. Brataas, G. E. W. Bauer, *Phys. Rev. Lett.* **2002**, *88*, 117601.

[28] H. Liu, C. Zhang, H. Malissa, M. Groesbeck, M. Kavand, R. McLaughlin, S. Jamali, J. Hao, D. Sun, R. A. Davidson, L. Wojcik, J. S. Miller, C. Boehme, Z. V. Vardeny, *Nat. Mater.* **2018**, *17*, 308.

[29] L. Guo, Y. Qin, X. Gu, X. Zhu, Q. Zhou, X. Sun, *Front. Chem.* **2019**, *7*, 428.

[30] K. Iniewski, *Nano-Semiconductors: Devices and Technology*, Taylor & Francis, London **2011**.

[31] S. Sanvito, *Nat. Mater.* **2007**, *6*, 803.

[32] H.-J. Jang, C. A. Richter, *Adv. Mater.* **2017**, *29*, 1602739.

[33] M. Julliere, *Phys. Lett. A* **1975**, *54*, 225.

[34] K. Ando, S. Watanabe, S. Mooser, E. Saitoh, H. Sirringhaus, *Nat. Mater.* **2013**, *12*, 622.

[35] E. Saitoh, M. Ueda, H. Miyajima, G. Tatara, *Appl. Phys. Lett.* **2006**, *88*, 182509.

[36] S. Watanabe, K. Ando, K. Kang, S. Mooser, Y. Vaynzof, H. Kurebayashi, E. Saitoh, H. Sirringhaus, *Nat. Phys.* **2014**, *10*, 308.

[37] J. C. Rojas-Sánchez, N. Reyren, P. Laczkowski, W. Savero, J. P. Attané, C. Deranlot, M. Jamet, J. M. George, L. Vila, H. Jaffrès, *Phys. Rev. Lett.* **2014**, *112*, 106602.

[38] T. D. Nguyen, G. Hukic-Markosian, F. Wang, L. Wojcik, X.-G. Li, E. Ehrenfreund, Z. V. Vardeny, *Nat. Mater.* **2010**, *9*, 345.

[39] M. Cinchetti, K. Heimer, J.-P. Wüstenberg, O. Andreyev, M. Bauer, S. Lach, C. Ziegler, Y. Gao, M. Aeschlimann, *Nat. Mater.* **2009**, *8*, 115.

[40] A. J. Drew, J. Hoppler, L. Schulz, F. L. Pratt, P. Desai, P. Shakya, T. Kreouzis, W. P. Gillin, A. Suter, N. A. Morley, V. K. Malik, A. Dubroka, K. W. Kim, H. Bouyanfif, F. Bourqui, C. Bernhard, R. Scheuermann, G. J. Nieuwenhuys, T. Prokscha, E. Morenzoni, *Nat. Mater.* **2009**, *8*, 109.

[41] S. Reineke, F. Lindner, G. Schwartz, N. Seidler, K. Walzer, B. Lüssem, K. Leo, *Nature* **2009**, *459*, 234.

[42] K. Walzer, B. Maennig, M. Pfeiffer, K. Leo, *Chem. Rev.* **2007**, *107*, 1233.

[43] R. Timmreck, T. Meyer, J. Gilot, H. Seifert, T. Mueller, A. Furlan, M. M. Wienk, D. Wynands, J. Hohl-Ebinger, W. Warta, R. A. J. Janssen, M. Riede, K. Leo, *Nat. Photonics* **2015**, *9*, 478.

[44] S. Fratini, M. Nikolka, A. Salleo, G. Schweicher, H. Sirringhaus, *Nat. Mater.* **2020**, *19*, 491.

[45] H. Sirringhaus, *Adv. Mater.* **2014**, *26*, 1319.

[46] D. L. Cheung, A. Troisi, *Phys. Chem. Chem. Phys.* **2008**, *10*, 5941.

[47] A. Troisi, *Chem. Soc. Rev.* **2011**, *40*, 2347.

[48] A. Privitera, R. Warren, G. Londi, P. Kaienburg, J. Liu, A. Sperlich, A. E. Lauritzen, O. Thimm, A. Ardavan, D. Beljonne, M. Riede, *J. Mater. Chem. C* **2021**, *9*, 2944.

[49] M. Schwarze, W. Tress, B. Beyer, F. Gao, R. Scholz, C. Poelking, K. Ortstein, A. A. Günther, D. Kasemann, D. Andrienko, K. Leo, *Science* **2016**, *352*, 1446.

[50] A. Privitera, G. Londi, M. Riede, G. D'Avino, D. Beljonne, *Adv. Funct. Mater.* **2020**, *30*, 2004600.

[51] R. Warren, A. Privitera, P. Kaienburg, A. E. Lauritzen, O. Thimm, J. Nelson, M. K. Riede, *Nat. Commun.* **2019**, *10*, 5538.

[52] S. Schott, U. Chopra, V. Lemaur, A. Melnyk, Y. Olivier, R. Di Pietro, I. Romanov, R. L. Carey, X. Jiao, C. Jellett, M. Little, A. Marks, C. R. McNeill, I. McCulloch, E. R. McNellis, D. Andrienko, D. Beljonne, J. Sinova, H. Sirringhaus, *Nat. Phys.* **2019**, *15*, 814.

[53] Z. G. Yu, *Nat. Commun.* **2014**, *5*, 4842.

[54] S.-J. Wang, D. Venkateshvaran, M. R. Mahani, U. Chopra, E. R. McNellis, R. Di Pietro, S. Schott, A. Wittmann, G. Schweicher, M. Cubukcu, K. Kang, R. Carey, T. J. Wagner, J. N. M. Siebrecht, D. P. G. H. Wong, I. E. Jacobs, R. O. Abolǰadayel, A. Ionescu, S. A. Egorov, S. Mueller, O. Zadvorna, P. Skalski, C. Jellett, M. Little, A. Marks, I. McCulloch, J. Wunderlich, J. Sinova, H. Sirringhaus, *Nat. Electron.* **2019**, *2*, 98.

[55] Z. G. Yu, *Phys. Rev. B* **2012**, *85*, 115201.

[56] G. A. H. Wetzelaer, L. J. A. Koster, P. W. M. Blom, *Phys. Rev. Lett.* **2011**, *107*, 066605.

[57] S. Schott, E. R. McNellis, C. B. Nielsen, H.-Y. Chen, S. Watanabe, H. Tanaka, I. McCulloch, K. Takimiya, J. Sinova, H. Sirringhaus, *Nat. Commun.* **2017**, *8*, 15200.

[58] S. Pramanik, C. G. Stefanita, S. Patibandla, S. Bandyopadhyay, K. Garre, N. Harth, M. Cahay, *Nat. Nanotechnol.* **2007**, *2*, 216.

[59] R. J. Elliott, *Phys. Rev.* **1954**, *96*, 266.

[60] Y. Sheng, T. D. Nguyen, G. Veeraraghavan, Ö. Mermer, M. Wohlgenannt, *Phys. Rev. B* **2007**, *75*, 035202.

[61] L. Nuccio, M. Willis, L. Schulz, S. Fratini, F. Messina, M. D'Amico, F. L. Pratt, J. S. Lord, I. McKenzie, M. Loth, B. Purushothaman, J. Anthony, M. Heeney, R. M. Wilson, I. Hernández, M. Cannas, K. Sedlak, T. Kreouzis, W. P. Gillin, C. Bernhard, A. J. Drew, *Phys. Rev. Lett.* **2013**, *110*, 216602.

[62] M. I. D'yakonov, V. I. Perel', *Sov. J. Exp. Theor. Phys.* **1971**, *33*, 1053.

[63] G. L. Bir, A. G. Aronov, G. E. Pikus, *JETP* **1975**, *42*, 705.

[64] T. D. Nguyen, E. Ehrenfreund, Z. V. Vardeny, *Science* **2012**, *337*, 204.

[65] Z. G. Yu, F. Ding, H. Wang, *Phys. Rev. B* **2013**, *87*, 205446.

[66] J. Takeya, M. Yamagishi, Y. Tominari, R. Hirahara, Y. Nakazawa, T. Nishikawa, T. Kawase, T. Shimoda, S. Ogawa, *Appl. Phys. Lett.* **2007**, *90*, 102120.

[67] Y. Yuan, G. Giri, A. L. Ayzner, A. P. Zoombelt, S. C. B. Mannsfeld, J. Chen, D. Nordlund, M. F. Toney, J. Huang, Z. Bao, *Nat. Commun.* **2014**, *5*, 3005.

[68] H. Minemawari, T. Yamada, H. Matsui, J. Tsutsumi, S. Haas, R. Chiba, R. Kumai, T. Hasegawa, *Nature* **2011**, *475*, 364.

[69] C. Mitsui, T. Okamoto, M. Yamagishi, J. Tsurumi, K. Yoshimoto, K. Nakahara, J. Soeda, Y. Hirose, H. Sato, A. Yamano, T. Uemura, J. Takeya, *Adv. Mater.* **2014**, *26*, 4546.

[70] V. Podzorov, E. Menard, J. A. Rogers, M. E. Gershenson, *Phys. Rev. Lett.* **2005**, *95*, 226601.

[71] T. Uemura, K. Nakayama, Y. Hirose, J. Soeda, M. Uno, W. Li, M. Yamagishi, Y. Okada, J. Takeya, *Curr. Appl. Phys.* **2012**, *12*, S87.

[72] H. Yada, R. Uchida, H. Sekine, T. Terashige, S. Tao, Y. Matsui, N. Kida, S. Fratini, S. Ciuchi, Y. Okada, T. Uemura, J. Takeya, H. Okamoto, *Appl. Phys. Lett.* **2014**, *105*, 143302.

[73] Z. Q. Li, V. Podzorov, N. Sai, M. C. Martin, M. E. Gershenson, M. Di Ventra, D. N. Basov, *Phys. Rev. Lett.* **2007**, *99*, 016403.

[74] S. Fratini, D. Mayou, S. Ciuchi, *Adv. Funct. Mater.* **2016**, *26*, 2292.

[75] G. Schweicher, G. D'Avino, M. T. Ruggiero, D. J. Harkin, K. Broch, D. Venkateshvaran, G. Liu, A. Richard, C. Ruzié, J. Armstrong, A. R. Kennedy, K. Shankland, K. Takimiya, Y. H. Geerts, J. A. Zeitler, S. Fratini, H. Sirringhaus, *Adv. Mater.* **2019**, *31*, 1902407.

[76] J. Tsurumi, H. Matsui, T. Kubo, R. Häusermann, C. Mitsui, T. Okamoto, S. Watanabe, J. Takeya, *Nat. Phys.* **2017**, *13*, 994.

[77] Z. H. Xiong, D. Wu, Z. Valy Vardeny, J. Shi, *Nature* **2004**, *427*, 821.

[78] X. Sun, M. Gobbi, A. Bedoya-Pinto, O. Txoperena, F. Golmar, R. Llopis, A. Chuvilin, F. Casanova, L. E. Hueso, *Nat. Commun.* **2013**, *4*, 2794.

[79] H. H. Choi, A. F. Paterson, M. A. Fusella, J. Panidi, O. Solomeshch, N. Tessler, M. Heeney, K. Cho, T. D. Anthopoulos, B. P. Rand, V. Podzorov, *Adv. Funct. Mater.* **2020**, *30*, 1903617.

[80] J. W. Orton, M. J. Powell, *Rep. Prog. Phys.* **1980**, *43*, 1263.

[81] H. Matsui, D. Kumaki, E. Takahashi, K. Takimiya, S. Tokito, T. Hasegawa, *Phys. Rev. B* **2012**, *85*, 035308.

[82] F. Zhao, C. Wang, X. Zhan, *Adv. Energy Mater.* **2018**, *8*, 1703147.

[83] X. Sun, A. Bedoya-Pinto, Z. Mao, M. Gobbi, W. Yan, Y. Guo, A. Atxabal, R. Llopis, G. Yu, Y. Liu, A. Chuvilin, F. Casanova, L. E. Hueso, *Adv. Mater.* **2016**, *28*, 2609.

[84] C. B. Nielsen, M. Turbiez, I. McCulloch, *Adv. Mater.* **2013**, *25*, 1859.

[85] A. Devižis, K. Meerholz, D. Hertel, V. Gulbinas, *Chem. Phys. Lett.* **2010**, *498*, 302.

[86] E. Hendry, M. Koeberg, J. M. Schins, H. K. Nienhuys, V. Sundström, L. D. A. Siebbeles, M. Bonn, *Phys. Rev. B* **2005**, *71*, 125201.

[87] P. Prins, F. C. Grozema, J. M. Schins, S. Patil, U. Scherf, L. D. A. Siebbeles, *Phys. Rev. Lett.* **2006**, *96*, 146601.

[88] R. Noriega, J. Rivnay, K. Vandewal, F. P. V. Koch, N. Stingelin, P. Smith, M. F. Toney, A. Salleo, *Nat. Mater.* **2013**, *12*, 1038.

[89] S. A. Mollinger, B. A. Krajina, R. Noriega, A. Salleo, A. J. Spakowitz, *ACS Macro Lett.* **2015**, *4*, 708.

[90] L. H. Jimison, M. F. Toney, I. McCulloch, M. Heeney, A. Salleo, *Adv. Mater.* **2009**, *21*, 1568.

[91] L. Guo, X. Gu, X. Zhu, X. Sun, *Adv. Mater.* **2019**, *31*, 1805355.

[92] W. J. M. Naber, S. Faez, W. G. van der Wiel, *J. Phys. D: Appl. Phys.* **2007**, *40*, R205.

[93] L. E. Hueso, I. Bergenti, A. Riminucci, Y. Q. Zhan, V. Dediu, *Adv. Mater.* **2007**, *19*, 2639.

[94] J. H. Park, E. Vescovo, H. J. Kim, C. Kwon, R. Ramesh, T. Venkatesan, *Nature* **1998**, *392*, 794.

[95] M. Bowen, M. Bibes, A. Barthélémy, J.-P. Contour, A. Anane, Y. Lemaître, A. Fert, *Appl. Phys. Lett.* **2003**, *82*, 233.

[96] F. J. Wang, C. G. Yang, Z. V. Vardeny, X. G. Li, *Phys. Rev. B* **2007**, *75*, 245324.

[97] A. Kahn, *Mater. Horiz.* **2016**, *3*, 7.

[98] H.-J. Jang, J.-S. Lee, S. J. Pookpanratana, C. A. Hacker, I. C. Tran, C. A. Richter, *J. Phys. Chem. C* **2015**, *119*, 12949.

[99] J. M. Manriquez, G. T. Yee, R. S. McLean, A. J. Epstein, J. S. Miller, *Science* **1991**, *252*, 1415.

[100] B. Li, C.-Y. Kao, J.-W. Yoo, V. N. Prigodin, A. J. Epstein, *Adv. Mater.* **2011**, *23*, 3382.

[101] A. Banerjee, A. J. Pal, *Small* **2018**, *14*, 1801510.

[102] M. Prezioso, A. Riminucci, I. Bergenti, P. Graziosi, D. Brunel, V. A. Dediu, *Adv. Mater.* **2011**, *23*, 1371.

[103] S. W. Jiang, B. B. Chen, P. Wang, Y. Zhou, Y. J. Shi, F. J. Yue, H. F. Ding, D. Wu, *Appl. Phys. Lett.* **2014**, *104*, 262402.

[104] R. Göckeritz, N. Homonnay, A. Müller, B. Fuhrmann, G. Schmidt, *AIP Adv.* **2016**, *6*, 045003.

[105] D. Sun, M. Fang, X. Xu, L. Jiang, H. Guo, Y. Wang, W. Yang, L. Yin, P. C. Snijders, T. Z. Ward, Z. Gai, X. G. Zhang, H. N. Lee, J. Shen, *Nat. Commun.* **2014**, *5*, 4396.

[106] K. Ando, S. Takahashi, J. Ieda, Y. Kajiwara, H. Nakayama, T. Yoshino, K. Harii, Y. Fujikawa, M. Matsuo, S. Maekawa, E. Saitoh, *J. Appl. Phys.* **2011**, *109*, 103913.

[107] D. Sun, K. J. van Schooten, M. Kavand, H. Malissa, C. Zhang, M. Groesbeck, C. Boehme, Z. Valy Vardeny, *Nat. Mater.* **2016**, *15*, 863.

[108] J. Niklas, S. Beaupré, M. Leclerc, T. Xu, L. Yu, A. Sperlich, V. Dyakonov, O. G. Poluektov, *J. Phys. Chem. B* **2015**, *119*, 7407.

[109] J. Niklas, O. G. Poluektov, *Adv. Energy Mater.* **2017**, *7*, 1602226.

[110] T. Biskup, *Front. Chem.* **2019**, *7*, 10.

[111] G. Szulczewski, S. Sanvito, M. Coey, *Nat. Mater.* **2009**, *8*, 693.

[112] M. B. Zimmt, C. Doubleday, N. J. Turro, *J. Am. Chem. Soc.* **1985**, *107*, 6726.

[113] E. L. Frankevich, I. A. Sokolik, *Solid State Commun.* **1970**, *8*, 251.

[114] E. L. Frankevich, A. A. Lymarev, I. Sokolik, F. E. Karasz, S. Blumstengel, R. H. Baughman, H. H. Hörhold, *Phys. Rev. B* **1992**, *46*, 9320.

[115] J. Kalinowski, J. Szmytkowski, W. Stampor, *Chem. Phys. Lett.* **2003**, *378*, 380.

[116] F. Ito, T. Ikoma, K. Akiyama, Y. Kobori, S. Tero-Kubota, *J. Am. Chem. Soc.* **2003**, *125*, 4722.

[117] F. Ito, T. Ikoma, K. Akiyama, A. Watanabe, S. Tero-Kubota, *J. Phys. Chem. B* **2005**, *109*, 8707.

[118] Z. Xu, B. Hu, J. Howe, *J. Appl. Phys.* **2008**, *103*, 043909.

[119] Z. Xu, B. Hu, *Adv. Funct. Mater.* **2008**, *18*, 2611.

[120] M. Shao, L. Yan, M. Li, I. Ilia, B. Hu, *J. Mater. Chem. C* **2013**, *1*, 1330.

[121] M. Wittmer, I. Zschokke-Gränacher, *J. Chem. Phys.* **1975**, *63*, 4187.

[122] M. Kotova, G. Londi, J. Junker, S. Dietz, A. Privitera, K. Tvingstedt, D. Beljonne, A. Sperlich, V. Dyakonov, *Mater. Horiz.* **2020**, *7*, 1641.

[123] N. Sharma, M. Y. Wong, D. Hall, E. Spuling, F. Tenopala-Carmona, A. Privitera, G. Copley, D. B. Cordes, A. M. Z. Slawin, C. Murawski, M. C. Gather, D. Beljonne, Y. Olivier, I. D. W. Samuel, E. Zysman-Colman, *J. Mater. Chem. C* **2020**, *8*, 3773.

[124] M. Righetto, F. Carraro, A. Privitera, G. Marafon, A. Moretto, C. Ferrante, *J. Phys. Chem. C* **2020**, *124*, 22314.

[125] A. Privitera, M. Righetto, D. Mosconi, F. Lorandi, A. A. Isse, A. Moretto, R. Bozio, C. Ferrante, L. Franco, *Phys. Chem. Chem. Phys.* **2016**, *18*, 31286.

[126] W. Han, R. K. Kawakami, M. Gmitra, J. Fabian, *Nat. Nanotechnol.* **2014**, *9*, 794.

[127] F. Kuemmeth, H. O. H. Churchill, P. K. Herring, C. M. Marcus, *Mater. Today* **2010**, *13*, 18.

[128] J. S. Manser, M. I. Saidaminov, J. A. Christians, O. M. Bakr, P. V. Kamat, *Acc. Chem. Res.* **2016**, *49*, 330.

[129] A. Babayigit, A. Ethirajan, M. Muller, B. Conings, *Nat. Mater.* **2016**, *15*, 247.

[130] D. Giovanni, M. Righetto, Q. Zhang, J. W. M. Lim, S. Ramesh, T. C. Sum, *Light: Sci. Appl.* **2021**, *10*, 2.

[131] M. Righetto, S. S. Lim, D. Giovanni, J. W. M. Lim, Q. Zhang, S. Ramesh, Y. K. E. Tay, T. C. Sum, *Nat. Commun.* **2020**, *11*, 2712.

[132] G. Xing, N. Mathews, S. Sun, S. S. Lim, Y. M. Lam, M. Grätzel, S. Mhaisalkar, T. C. Sum, *Science* **2013**, *342*, 344.

[133] T. C. Sum, M. Righetto, S. S. Lim, *J. Chem. Phys.* **2020**, *152*, 130901.

[134] J. Shamsi, A. S. Urban, M. Imran, L. De Trizio, L. Manna, *Chem. Rev.* **2019**, *119*, 3296.

[135] Y. Rakita, O. Bar-Elli, E. Meirzadeh, H. Kaslasi, Y. Peleg, G. Hodes, I. Lubomirsky, D. Oron, D. Ehre, D. Cahen, *Proc. Natl. Acad. Sci. USA* **2017**, *114*, E5504.

[136] A. Poglitsch, D. Weber, *J. Chem. Phys.* **1987**, *87*, 6373.

[137] J. Yin, P. Maity, L. Xu, A. M. El-Zohry, H. Li, O. M. Bakr, J.-L. Brédas, O. F. Mohammed, *Chem. Mater.* **2018**, *30*, 8538.

[138] J. Even, L. Pedesseau, J.-M. Jancu, C. Katan, *J. Phys. Chem. Lett.* **2013**, *4*, 2999.

[139] M. Kim, J. Im, A. J. Freeman, J. Ihm, H. Jin, *Proc. Natl. Acad. Sci. USA* **2014**, *111*, 6900.

[140] G. Dresselhaus, *Phys. Rev.* **1955**, *100*, 580.

[141] A. Manchon, H. C. Koo, J. Nitta, S. M. Frolov, R. A. Duine, *Nat. Mater.* **2015**, *14*, 871.

[142] M. Kepenekian, R. Robles, C. Katan, D. Sapori, L. Pedesseau, J. Even, *ACS Nano* **2015**, *9*, 11557.

[143] W. A. Dunlap-Shohl, Y. Zhou, N. P. Padture, D. B. Mitzi, *Chem. Rev.* **2019**, *119*, 3193.

[144] B. Wu, H. Yuan, Q. Xu, J. A. Steele, D. Giovanni, P. Puech, J. Fu, Y. F. Ng, N. F. Jamaludin, A. Solanki, S. Mhaisalkar, N. Mathews, M. B. J. Roeffaers, M. Grätzel, J. Hofkens, T. C. Sum, *Nat. Commun.* **2019**, *10*, 484.

[145] F. Zheng, L. Z. Tan, S. Liu, A. M. Rappe, *Nano Lett.* **2015**, *15*, 7794.

[146] L. Leppert, S. E. Reyes-Lillo, J. B. Neaton, *J. Phys. Chem. Lett.* **2016**, *7*, 3683.

[147] D. Niesner, M. Wilhelm, I. Levchuk, A. Osvet, S. Shrestha, M. Batentschuk, C. Brabec, T. Fauster, *Phys. Rev. Lett.* **2016**, *117*, 126401.

[148] T. Wang, B. Daiber, J. M. Frost, S. A. Mann, E. C. Garnett, A. Walsh, B. Ehrler, *Energy Environ. Sci.* **2017**, *10*, 509.

[149] T. Etienne, E. Mosconi, F. De Angelis, *J. Phys. Chem. Lett.* **2016**, *7*, 1638.

[150] O. Yaffe, Y. Guo, L. Z. Tan, D. A. Egger, T. Hull, C. C. Stoumpos, F. Zheng, T. F. Heinz, L. Kronik, M. G. Kanatzidis, J. S. Owen, A. M. Rappe, M. A. Pimenta, L. E. Brus, *Phys. Rev. Lett.* **2017**, *118*, 136001.

[151] J. M. Frost, K. T. Butler, A. Walsh, *APL Mater.* **2014**, *2*, 081506.

[152] I.-H. Park, Q. Zhang, K. C. Kwon, Z. Zhu, W. Yu, K. Leng, D. Giovanni, H. S. Choi, I. Abdelwahab, Q.-H. Xu, T. C. Sum, K. P. Loh, *J. Am. Chem. Soc.* **2019**, *141*, 15972.

[153] Y. Zhai, S. Baniya, C. Zhang, J. Li, P. Haney, C.-X. Sheng, E. Ehrenfreund, Z. V. Vardeny, *Sci. Adv.* **2017**, *3*, e1700704.

[154] J. Even, L. Pedesseau, J.-M. Jancu, C. Katan, *Phys. Status Solidi RRL* **2014**, *8*, 31.

2100215 (18 of 20)

[155] J. Even, L. Pedesseau, M. A. Dupertuis, J. M. Jancu, C. Katan, *Phys. Rev. B* **2012**, *86*, 205301.

[156] J. Even, L. Pedesseau, C. Katan, *J. Phys. Chem. C* **2014**, *118*, 11566.

[157] D. Giovanni, H. Ma, J. Chua, M. Grätzel, R. Ramesh, S. Mhaisalkar, N. Mathews, T. C. Sum, *Nano Lett.* **2015**, *15*, 1553.

[158] P. C. Sercel, J. L. Lyons, D. Wickramaratne, R. Vaxenburg, N. Bernstein, A. L. Efros, *Nano Lett.* **2019**, *19*, 4068.

[159] S. Strohmair, A. Dey, Y. Tong, L. Polavarapu, B. J. Bohn, J. Feldmann, *Nano Lett.* **2020**, *20*, 4724.

[160] D. Giovanni, W. K. Chong, Y. Y. F. Liu, H. A. Dewi, T. Yin, Y. Lekina, Z. X. Shen, N. Mathews, C. K. Gan, T. C. Sum, *Adv. Sci.* **2018**, *5*, 1800664.

[161] D. Giovanni, J. W. M. Lim, Z. Yuan, S. S. Lim, M. Righetto, J. Qing, Q. Zhang, H. A. Dewi, F. Gao, S. G. Mhaisalkar, N. Mathews, T. C. Sum, *Nat. Commun.* **2019**, *10*, 3456.

[162] P. Odenthal, W. Talmadge, N. Gundlach, R. Wang, C. Zhang, D. Sun, Z.-G. Yu, Z. Valy Vardeny, Y. S. Li, *Nat. Phys.* **2017**, *13*, 894.

[163] V. V. Belykh, D. R. Yakovlev, M. M. Glazov, P. S. Grigoryev, M. Hussain, J. Rautert, D. N. Dirin, M. V. Kovalenko, M. Bayer, *Nat. Commun.* **2019**, *10*, 673.

[164] M. A. Becker, R. Vaxenburg, G. Nedelcu, P. C. Sercel, A. Shabaev, M. J. Mehl, J. G. Michopoulos, S. G. Lambrakos, N. Bernstein, J. L. Lyons, T. Stöferle, R. F. Mahrt, M. V. Kovalenko, D. J. Norris, G. Rainò, A. L. Efros, *Nature* **2018**, *553*, 189.

[165] M. Fu, P. Tamarat, H. Huang, J. Even, A. L. Rogach, B. Lounis, *Nano Lett.* **2017**, *17*, 2895.

[166] J. Liu, F. Hu, Y. Zhou, C. Zhang, X. Wang, M. Xiao, *J. Lumin.* **2020**, *221*, 117032.

[167] M. Shrivastava, M. I. Bodnarchuk, A. Hazarika, J. M. Luther, M. C. Beard, M. V. Kovalenko, K. V. Adarsh, *Adv. Opt. Mater.* **2020**, *8*, 2001016.

[168] Y. Li, X. Luo, Y. Liu, X. Lu, K. Wu, *ACS Energy Lett.* **2020**, *5*, 1701.

[169] M. J. Crane, L. M. Jacoby, T. A. Cohen, Y. Huang, C. K. Luscombe, D. R. Gamelin, *Nano Lett.* **2020**, *20*, 8626.

[170] T. T. H. Do, A. Granados del Águila, D. Zhang, J. Xing, S. Liu, M. A. Prosnikov, W. Gao, K. Chang, P. C. M. Christianen, Q. Xiong, *Nano Lett.* **2020**, *20*, 5141.

[171] D. Giovanni, W. K. Chong, H. A. Dewi, K. Thirumal, I. Neogi, R. Ramesh, S. Mhaisalkar, N. Mathews, T. C. Sum, *Sci. Adv.* **2016**, *2*, e1600477.

[172] K. Tanaka, T. Takahashi, T. Kondo, K. Umeda, K. Ema, T. Umebayashi, K. Asai, K. Uchida, N. Miura, *Jpn. J. Appl. Phys.* **2005**, *44*, 5923.

[173] X. Chen, H. Lu, Z. Li, Y. Zhai, P. F. Ndione, J. J. Berry, K. Zhu, Y. Yang, M. C. Beard, *ACS Energy Lett.* **2018**, *3*, 2273.

[174] M. Zhou, J. S. Sarmiento, C. Fei, X. Zhang, H. Wang, *J. Phys. Chem. Lett.* **2020**, *11*, 1502.

[175] S. B. Todd, D. B. Riley, A. Binai-Motlagh, C. Clegg, A. Ramachandran, S. A. March, J. M. Hoffman, I. G. Hill, C. C. Stoumpos, M. G. Kanatzidis, Z.-G. Yu, K. C. Hall, *APL Mater.* **2019**, *7*, 081116.

[176] S. A. Bourelle, R. Shivanna, F. V. A. Camargo, S. Ghosh, A. J. Gillett, S. P. Senanayak, S. Feldmann, L. Eyre, A. Ashoka, T. W. J. van de Goor, H. Abolins, T. Winkler, G. Cerullo, R. H. Friend, F. Deschler, *Nano Lett.* **2020**, *20*, 5678.

[177] M. Z. Maialle, E. A. de Andrada e Silva, L. J. Sham, *Phys. Rev. B* **1993**, *47*, 15776.

[178] S. D. Stranks, R. L. Z. Hoye, D. Di, R. H. Friend, F. Deschler, *Adv. Mater.* **2019**, *31*, 1803336.

[179] H. Zeng, J. Dai, W. Yao, D. Xiao, X. Cui, *Nat. Nanotechnol.* **2012**, *7*, 490.

[180] G. Engels, J. Lange, T. Schäpers, H. Lüth, *Phys. Rev. B* **1997**, *55*, R1958.

[181] J. Nitta, T. Akazaki, H. Takayanagi, T. Enoki, *Phys. Rev. Lett.* **1997**, *78*, 1335.

[182] Y. Yang, S. Feng, Z. Li, T. Li, Y. Xiong, L. Cao, X. Gao, *J. Phys. Chem. Lett.* **2019**, *10*, 4422.

[183] K. Ando, S. Takahashi, J. Ieda, H. Kurebayashi, T. Trypiniotis, C. H. W. Barnes, S. Maekawa, E. Saitoh, *Nat. Mater.* **2011**, *10*, 655.

[184] G. Schmidt, D. Ferrand, L. W. Molenkamp, A. T. Filip, B. J. van Wees, *Phys. Rev. B* **2000**, *62*, R4790.

[185] J. Wang, C. Zhang, H. Liu, R. McLaughlin, Y. Zhai, S. R. Vardeny, X. Liu, S. McGill, D. Semenov, H. Guo, R. Tsuchikawa, V. V. Deshpande, D. Sun, Z. V. Vardeny, *Nat. Commun.* **2019**, *10*, 129.

[186] X. Liu, A. Chanana, U. Huynh, F. Xue, P. Haney, S. Blair, X. Jiang, Z. V. Vardeny, *Nat. Commun.* **2020**, *11*, 323.

[187] M. Li, J. Fu, Q. Xu, T. C. Sum, *Adv. Mater.* **2019**, *31*, 1802486.

[188] J. Li, P. M. Haney, *Appl. Phys. Lett.* **2016**, *109*, 193903.

[189] D. Niesner, M. Hauck, S. Shrestha, I. Levchuk, G. J. Matt, A. Osvet, M. Batentschuk, C. Brabec, H. B. Weber, T. Fauster, *Proc. Natl. Acad. Sci. USA* **2018**, *115*, 9509.

[190] P. A. Obraztsov, D. Lyashenko, P. A. Chizhov, K. Konishi, N. Nemoto, M. Kuwata-Gonokami, E. Welch, A. N. Obraztsov, A. Zakhidov, *Commun. Phys.* **2018**, *1*, 14.

[191] S. D. Ganichev, E. L. Ivchenko, V. V. Bel'kov, S. A. Tarasenko, M. Sollinger, D. Weiss, W. Wegscheider, W. Prettl, *Nature* **2002**, *417*, 153.

[192] W. Li, L. Zhou, O. V. Prezhdo, A. V. Akimov, *ACS Energy Lett.* **2018**, *3*, 2159.

[193] W. Qin, H. Xu, B. Hu, *ACS Photonics* **2017**, *4*, 2821.

[194] A. Gusain, A. Thankappan, S. Thomas, *J. Mater. Sci.* **2020**, *55*, 13490.

[195] M. Cinchetti, V. A. Dediu, L. E. Hueso, *Nat. Mater.* **2017**, *16*, 507.

[196] V. Dediu, L. E. Hueso, I. Bergenti, A. Riminucci, F. Borgatti, P. Graziosi, F. Newby, F. Casoli, M. P. De Jong, C. Taliani, Y. Zhan, *Phys. Rev. B* **2008**, *78*, 115203.

[197] X. Lou, C. Adelmann, S. A. Crooker, E. S. Garlid, J. Zhang, K. S. M. Reddy, S. D. Flexner, C. J. Palmstrøm, P. A. Crowell, *Nat. Phys.* **2007**, *3*, 197.

[198] A. Riminucci, M. Prezioso, C. Pernechele, P. Graziosi, I. Bergenti, R. Cecchini, M. Calbucci, M. Solzi, V. A. Dediu, *Appl. Phys. Lett.* **2013**, *102*, 092407.

[199] M. Grünewald, R. Göckeritz, N. Homonnay, F. Würthner, L. W. Molenkamp, G. Schmidt, *Phys. Rev. B* **2013**, *88*, 085319.

[200] Z. G. Yu, *Phys. Rev. Lett.* **2013**, *111*, 016601.

[201] S. Yang, E. Vetter, T. Wang, A. Amassian, D. Sun, *J. Phys.: Mater.* **2020**, *3*, 015012.

[202] X. Pan, H. Liu, U. Huynh, Z. V. Vardeny, *J. Chem. Phys.* **2020**, *152*, 044714.

[203] R. Naaman, Y. Paltiel, D. H. Waldeck, *Nat. Rev. Chem.* **2019**, *3*, 250.

[204] G. Long, R. Sabatini, M. I. Saidaminov, G. Lakhwani, A. Rasmita, X. Liu, E. H. Sargent, W. Gao, *Nat. Rev. Mater.* **2020**, *5*, 423.

[205] J. Ahn, S. Ma, J.-Y. Kim, J. Kyhm, W. Yang, J. A. Lim, N. A. Kotov, J. Moon, *J. Am. Chem. Soc.* **2020**, *142*, 4206.

[206] M. K. Jana, R. Song, H. Liu, D. R. Khanal, S. M. Janke, R. Zhao, C. Liu, Z. Valy Vardeny, V. Blum, D. B. Mitzi, *Nat. Commun.* **2020**, *11*, 4699.

[207] H. Lu, J. Wang, C. Xiao, X. Pan, X. Chen, R. Brunecky, J. J. Berry, K. Zhu, M. C. Beard, Z. V. Vardeny, *Sci. Adv.* **2019**, *5*, eaay0571.

[208] A. Privitera, M. Righetto, F. De Bastiani, F. Carraro, M. Rancan, L. Armelao, G. Granozzi, R. Bozio, L. Franco, *J. Phys. Chem. Lett.* **2017**, *8*, 5981.

[209] M. Righetto, D. Meggiolaro, A. Rizzo, R. Sorrentino, Z. He, G. Meneghesso, T. C. Sum, T. Gatti, F. Lamberti, *Prog. Mater. Sci.* **2020**, *110*, 100639.

Alberto Privitera received his Ph.D. in materials science at the University of Padova. The focus of his thesis was on the investigation of electron spin states in nanostructured materials for organic and hybrid solar cells. After his Ph.D., he joined the research group of Prof. Riede at the University of Oxford where he has contributed to disclose the role of spin-bearing species and their interactions in organic optoelectronics. Currently, he is a postdoctoral researcher in the EPR group of the University of Turin where he is focusing on the chiral-induced spin selectivity (CISS) effect.

Marcello Righetto received his M.Sc. (2014) and Ph.D. (2018) in materials science at the University of Padova, where his research focused on quantum-confined semiconductors. Before moving to University College London (UCL) as a research fellow in Prof. Cacialli's lab, he worked for two years at Nanyang Technological University (NTU), where his research focused on halide perovskites. Currently, his research at UCL focuses on halide perovskite and organic semiconductor optoelectronic devices.

Franco Cacialli is a professor of physics in the London Centre for Nanotechnology and the Department of Physics at University College London (UCL). His interests focus on the physics and application of organic and printable semiconductors to optoelectronics. A former Royal Society University research fellow, he coordinated two Marie Curie Research Training Networks on threaded molecular wires (http://www.threadmill-rtn.eu) and on supramolecular materials for photonics (synchronics-etn.eu). A fellow of the Institute of Physics (2001), of the American Physical Society (2009), and a recipient of a Royal Society Wolfson Research Merit Award (2015–2019), he is currently a codirector of the London Institute for Advanced Light Technologies (london-light.org).

Moritz K. Riede is a professor of soft functional nanomaterials in the Department of Physics at the University of Oxford, UK. Before moving to Oxford in 2013, he worked in Germany at the Technische Universität Dresden as postdoc and as head of a junior research group (2007–2013) with Prof. Karl Leo. His academic research focuses on organic semiconductors, in particular vacuum-processed organic solar cells that have potential to transform the way we use solar energy. In parallel to his research, he is active at the interface between science and society. He is alumnus and a past co-chair of the Global Young Academy.